sustainability

MDPI

Article

Spatiotemporal Analysis of Land Use/Land Cover and Its Effects on Surface Urban Heat Island Using Landsat Data: A Case Study of Metropolitan City Tehran (1988–2018)

Iman Rousta [1,2], Md Omar Sarif [3,*], Rajan Dev Gupta [4], Haraldur Olafsson [5], Manjula Ranagalage [6,7], Yuji Murayama [8], Hao Zhang [9,*] and Terence Darlington Mushore [10]

1 Department of Geography, Yazd University, Yazd 8915818411, Iran; irousta@yazd.ac.ir
2 Institute for Atmospheric Sciences, University of Iceland and Icelandic Meteorological Office (IMO), Bustadavegur 7, IS-108 Reykjavik, Iceland
3 Geographic Information System (GIS) Cell, Motilal Nehru National Institute of Technology Allahabad, Prayagraj 211004, India
4 Civil Engineering Department, and Member of GIS Cell, Motilal Nehru National Institute of Technology Allahabad, Prayagraj 211004, India; rdg@mnnit.ac.in
5 Department of Physics, University of Iceland, Institute for Atmospheric Sciences and Icelandic Meteorological Office (IMO), Bustadavegur 7, IS-108 Reykjavik, Iceland; haraldur68@gmail.com
6 Graduate School of Life and Environmental Sciences, University of Tsukuba 1-1-1, Tennodai, Tsukuba, Ibaraki 305-8572, Japan; manjularanagalage@gmail.com
7 Department of Environmental Management, Faculty of Social Sciences and Humanities, Rajarata University of Sri Lanka, Mihintale 50300, Sri Lanka
8 Faculty of Life and Environmental Sciences, University of Tsukuba, 1-1-1 Tennodai, Tsukuba City, Ibaraki 305-8572, Japan; mura@geoenv.tsukuba.ac.jp
9 Department of Environmental Science and Engineering Jiangwan campus, Fudan University, 2005 Songhu Road, Yangpu District, Shanghai 200438, China
10 Department of Physics, Faculty of Science, University of Zimbabwe, MP167 Mt Pleasant, Harare 00263, Zimbabwe; tdmushore@science.uz.ac.zw
* Correspondence: rgi1606@mnnit.ac.in (M.O.S.); zhokzhok@163.com (H.Z.)

Received: 30 October 2018; Accepted: 20 November 2018; Published: 27 November 2018

Abstract: This article summarized the spatiotemporal pattern of land use/land cover (LU/LC) and urban heat island (UHI) dynamics in the Metropolitan city of Tehran between 1988 and 2018. The study showed dynamics of each LU/LC class and their role in influencing the UHI. The impervious surface area expanded by 286.04 (48.27% of total land) and vegetated land was depleted by 42.06 km^2 (7.10% of total land) during the period of 1988–2018. The mean land surface temperature (LST) has enlarged by approximately 2–3 °C at the city center and 5–7 °C at the periphery between 1988 and 2018 based on the urban–rural gradient analysis. The lower mean LST was experienced by vegetation land (VL) and water body (WB) by approximately 4–5 °C and 5–7 °C, respectively, and the higher mean LST by open land (OL) by 7–11 °C than other LU/LC classes at all time-points during the time period, 1988–2018. The magnitude of mean LST was calculated based on the main LU/LC categories, where impervious land (IL) recorded the higher temperature difference compared to vegetation land (VL) and water bodies (WB). However, open land (OL) recorded the highest mean LST differences with all the other LU/LC categories. In addition to that, there was an overall negative correlation between LST and the normal difference vegetation index (NDVI). By contrast, there was an overall positive correlation between LST and the normal difference built-up index (NDBI). This article, executed through three decadal change analyses from 1988 to 2018 at 10-year intervals, has made a significant contribution to delineating the long records of change dynamics and could have a great influence on policy making to foster environmental sustainability.

Keywords: LU/LC dynamics; SUHI; LST; NDVI; NDBI; Tehran

1. Introduction

Globally, urban population has expanded to 54.5% (in 2016) and, if the trend persists, then the urban population will be 60% of the global total in 2030 [1]. The rapid alteration through impervious growth in the landscape of land use/land cover (LU/LC) directly or indirectly influences the local environment concerning its climatic variabilities, as well as economic perspectives [2]. The trend of transformation of natural landscape into urban settlements has led to a change in the confined environment, with high elevated temperature compared to its surroundings [3–5]. The observed higher temperature over the urban than the rural areas led to the creation of an urban heat island (UHI) [5,6]. This difference in temperature over urban–rural landscapes has been raised mainly because of the depletion of green space, shrinking of water bodies, lessening of farmland, and the growth of impervious surface [4,5,7].

The swift concern in LU/LC knowledge building has been developed in the recent past because this knowledge gives us the ability to explore urban ecology, morphology, geography, and sustainability through developing the idea of urban diversity, urban intensity, the pattern of land use, UHI phenomena, and others [2,5]. LU/LC not only largely influences a wide stream of urban planning, but also influences policy making, transportation network development, environmental enhancement, and economic growth [2]. LU/LC has been studied in two distinct ways in developing and developed nations, through urban growth and urban improvement, which further ascertains that LU/LC is a more crucial condition in developed nations compared to developing nations, as green enhanced environment space is complicated to establish in developed nations due to a lack of spatial space [2,3,8,9].

Cities inherit different properties of physical surfaces, which lead to a wide array of different surface behavior patterns regarding longwave radiation, the absorbance of electromagnetic radiation, evaporation, prevailing winds blockage, and the release of heat for human-made reasons [10]. The different materials of the urban physical surface differ widely, as they constitute the surface of asphalt, gravel, stones, pebbles, flooring, and concrete, which increase the sensitivity and decrease the evapotranspiration of the city. These are all heavily influencing the local climate of the city [4,8,11]. Consequently, cities are facing warmer weather than their peripheral areas or rural areas, and this phenomenon is called surface UHI (SUHI). SUHI is one of the significant influencing elements for drastic alterations in the scenario of the atmosphere of the local space, affecting the life of animals, including humans, and natural aspects (like macro- and microorganisms) [4,12–14]. SUHI is spreading over urban space in higher magnitudes of temperature compared to its surrounding suburban and rural space, which is mainly influenced by the high level of impervious land (IL) development or urbanization [15,16]. SUHI has strongly attracted the attention of policy makers, health authorities, urban planners, urban investors, and other different scientific communities due to its adverse effects on human health, as well as on environmental properties like air quality, precipitation, temperature, store carbon, energy balance, etc. [8,17,18].

Now, mitigation strategies need to be incorporated, and therefore the spatial dynamics of a city's landscape need to be understood to deal with the adverse effects of SUHI phenomena [10]. Essentially, properly designed building structures and environmentally friendly raw materials have been suggested in the recent past to cope with excessive impermeability, effective potentiality in solar radiance absorbance, and thermal energy storage. This can be helpful to develop an appropriate strategy towards thermal properties and produce the best suitable mitigation actions, like green roof and cool roof with energy balance, rainwater harvesting, etc., to overcome the SUHI effects [19]. Therefore, to quantify the LU/LC dynamics and SUHI phenomena, remote sensing (RS) and geographical information systems (GIS) technologies have been strongly recommended before, as these provide the most cost-effective and easiest ways to extract the actual scenario of the city in the context of spatiotemporal UHI with

LU/LC generations [6,20–26]. In a previous time, LU/LC dynamics were generated to obtain the quantized information about the land cover for the sake of sustainable development [2,8,27–34]. Previously, the relationship of land surface temperature (LST) vs. normal difference vegetation index (NDVI) [7,8,35–38], and LST vs. normal difference built-up index (NDBI) [39–41] have been taken into consideration to visualize the actual status of the local landscape [39,42,43].

In this article, spatiotemporal datasets of Landsat (1988–2018) have been thoroughly used for the analysis of the variation of LU/LC and SUHI dynamics phenomena over the city of Tehran using summer dry season (July–August) data. The reason behind choosing this study area is that this city is one of the most rapidly expanding cities in the Middle East. As a consequence, the LU/LC dynamics are very dramatically altered in its city center and the periphery, which directly or indirectly alters the land–resources dynamics. Therefore, timely intervention is the need of the hour for the sustainable development of Tehran.

The objectives of this article include: (i) To study the multitemporal spatial dynamics of LU/LC change and its effect towards SUHI generation for the metropolitan city of Tehran; (ii) to extract the mean LST of each LU/LC class and the change dynamics, along with their effect on the landscape of the city; (iii) to derive LU/LC indicators, such as NDVI and NDBI, to visualize the role of green space and impervious space on the surface temperature in the scenery of Tehran; (iv) to carry out urban–rural gradients analysis to observe the difference of temperature between vegetation vs. urban status and how these influence each other in the context of temperature on the local landscape level of Tehran.

2. Materials and Methods

2.1. Study Area: Tehran, Iran

Tehran, the capital city of Iran, is located in the northern part of this nation at the hillside location of the southern side of Alborz Mountains, and is spread over latitude 35°30′ to 35°51′ and longitude 51°00′ to 51°40′ [10,44,45] (Figure 1). It had a population of 0.21 million in 1921 [44]. Later, in 2016, it had a population of 8.52 million [1]. Now, it has become the most populous city in Iran [10,46]. It principally has two types of physiographic conditions: In the northern part, it has mountainous physiology, and in the southern part, it has a desert type of physiology, with an altitudinal variation of 900 m to 1800 m. The altitudinal variation leads to having distinct climatic conditions, as in the north, Tehran has a dry and cold climate, whereas in the south, it has a warm and dry climate [10]. Due to these variations in physiology and climatic conditions, Tehran has been experiencing an annual mean minimum of rainfall of 145 mm in the south and a maximum of 422 mm in the north, with an average of 33 days of rain in the south and 89 days of rain in the north [10], whereas in the context of annual mean temperature, it has been experiencing 15 °C to 18 °C and this range has been changing by 3 °C by altitudinal variation [10].

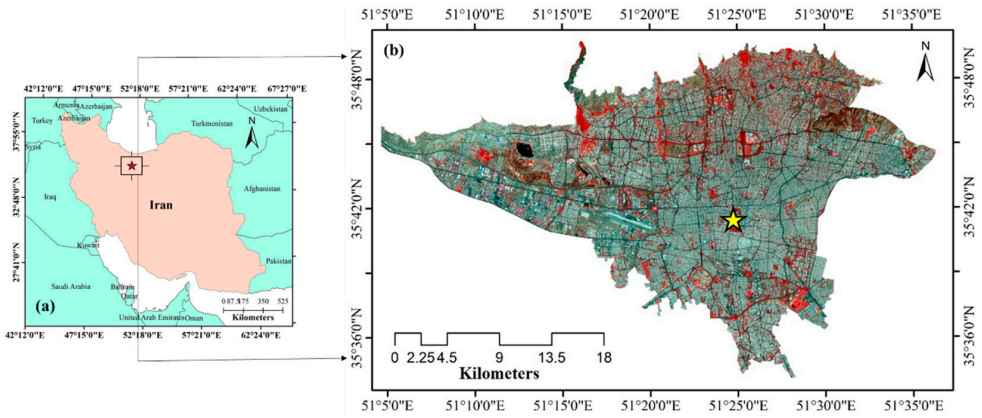

Figure 1. Study area, a metropolitan city, Tehran; (**a**) Tehran location in the Middle East and (**b**) false color composite image of Landsat 8 (Band 5, 4, 3) of 12 July 2018 of Tehran City (https://earthexplorer.usgs.gov/).

2.2. Satellite Images

In this analysis, for the execution of LU/LC dynamics, LST, NDVI, and NDBI, Landsat 5 Thematic Mapper (TM) of 1988 to 2008 and Landsat 8 OLI/ TRIS datasets of 2018 (Table 1) were acquired from the United States Geological Survey (USGS) portal. This dataset was preprocessed to overcome atmospheric conditions, distortion, and errors through atmospheric and radiometric correction, as these are the most suitable algorithms to get errorless satellite images [3,4,20,47,48]. In this analysis, 10-year intervals were followed to visualize the IL and its role in LST intensification, as its development of expansion needs time to occur at a large scale for a city; therefore, 10-year intervals were an excellent choice to see the difference of LU/LC dynamics, as well as SUHI phenomena.

Table 1. Details of Landsat datasets of the study area, Tehran, of the last three decades at 10-year intervals (1988–2018).

Sensor	Scene ID	Acquisition Date	Time (GMT)	Thermal Conversion Constant	
				K_1	K_2
Landsat-5 TM	LT04_L1TP_164035_19880717_20170208_01_T1	17 July 1988	06:37:12	671.62 (Band 6)	1284.30 (Band 6)
Landsat-5 TM	LT05_L1TP_164035_19980721_20171207_01_T1	21 July 1998	06:46:24	607.76 (Band 6)	1260.56 (Band 6)
Landsat-5 TM	LT05_L1TP_164035_20080801_20161030_01_T1	1 August 2008	06:54:26	607.76 (Band 6)	1260.56 (Band 6)
Landsat-8 OLI/TIRS	LC08_L1TP_164035_20180712_20180712_01_RT	12 July 2018	07:07:15	774.8853 (Band 10)	1321.0789 (Band 10)

2.3. LU/LC Retrieval

To retrieve the LU/LC information, satellite images were used for the four different time-points, i.e., 1988 (Landsat TM), 1998 (Landsat TM), 2008 (Landsat TM), and 2018 (Landsat 8), over the metropolitan city of Tehran. For this LU/LC classification, supervised classification based on the maximum likelihood algorithm in ERDAS IMAGINE 2014 software was used to delineate five distinct classes. These five classes are impervious land (IL), vegetation land (VL), water body (WB), farm land (FL), and open land (OL).

For the execution of the accuracy assessment of each LU/LC class, a stratified random sampling method was carried out to extract the LU/LC classification accuracy. For the assessment of accuracy, a total of 1000 points were selected by visual interpretation of each class from Landsat datasets of all four different time-points [10,40]. User accuracy, producer accuracy, overall accuracy, and lastly, the Kappa coefficient were calculated to indicate the level of classification accuracy [49–51]. Kappa is a nonparametric test which was used to find out the level of agreement between user-assigned values and predefined assigned values [52]. The accuracy test, called overall accuracy, user accuracy, producer accuracy, and the Kappa coefficient were performed using Equations (1)–(4) respectively [10,40]:

$$Overall\ Accuracy = \left\{ \frac{\sum CCP(Diagonal)}{\sum CRP} * 100 \right\}, \quad (1)$$

where $CCP(Diagonal)$ is the corrected classified pixels (diagonals) and CRP is the corrected reference pixels;

$$User\ Accuracy = \left\{ \frac{\sum CCP(Category)}{\sum CPC(Row)} * 100 \right\}, \quad (2)$$

where $CCP(Category)$ is the corrected classified pixels (category) and $CPC(Row)$ is the classified pixels in that category (the row total);

$$Producer\ Accuracy = \left\{ \frac{\sum CCP(Category)}{\sum CPC(Column)} * 100 \right\}, \quad (3)$$

where $CCP(Category)$ is the corrected classified pixels (diagonals) and $CPC(Column)$ is the classified pixels in that category (the column total);

$$Kappa\ Coefficients = \frac{N\sum_{i=1}^{r} X_{ii}\sum_{i=1}^{r}(X_{i+} * X_{+i})}{N^2 - \sum_{i=1}^{r}(X_{i+} * X_{+i})}, \quad (4)$$

where N is the total samples; r is the number of rows in error matrix; X_{ii} is the total corrected samples in ith row and column; N^2 is the square of total samples; X_{i+} is the column total; and X_{+i} is the row total.

2.4. Retrieval of LST

For the calculation of LST, first of all, the thermal band (Band 6 in Landsat TM, and Band 10 in Landsat 8) raw data were converted into spectral radiance values using Equation (5) [47]:

$$L_\varphi = M_L * Q_{Cal} + A_L, \quad (5)$$

where L_φ is top of atmosphere (TOA) spectral radiance (watts/(m^2 *sr*μm)), M_L is the multiplicative rescaling factor based on a specific band from the metadata, Q_{Cal} is the quantized and calibrated pixel values (digital number (DN)) of standard product, and A_L is the additive rescaling factor based on a specific band from the metadata.

Then, the at sensor (brightness) temperature value was extracted using Equation (6) [5,10,15,16,43,50,51]:

$$\tau = \left[\frac{K_2}{\ln\left(\frac{K_1}{L_\varphi} + 1\right)}\right], \quad (6)$$

where τ is At sensor brightness temperature, L_φ is the TOA spectral radiance (watts/(m^2 *sr*μm)), and K_1 and K_2 are the thermal conversion constants from the metadata (Band 6 for Landsat TM, and Band 10 for Landsat 8) (Table 2).

Now, with the help of emissivity correction using Equation (7), the LST (in Kelvin (K)) was derived from the brightness temperature [5,10,15,16,43,50,51]:

$$\omega = \left[\frac{\tau}{1 + w\left(\frac{\tau}{p}\right)\ln(e)}\right], \quad (7)$$

where τ is the At sensor temperature, w is the emitted radiance wavelength (11.5 μm for Band 6 in Landsat TM, and 10.8 μm for Band 10 in Landsat 8), $p = h \times c/s\ \left(1.438 \times 10^{-2}\ \text{mK}\right)$, h is Plank's constant (6.626×10^{-34} Js), s is the Boltzmann Constant (1.38×10^{-23} J/K), and c is the velocity of light (2.988×10^8 m/s).

Equation (8) was employed for the extraction of land surface emissivity (e) [5,10,15,16,43,50]:

$$e = n\ P_v + m, \quad (8)$$

where e is land surface emissivity, n = 0.004 [4] and m = 0.986 [4], and P_v is the proportion of vegetation.

Equation (9) was then incorporated for the extraction of the proportion of vegetation (P_v) [5,10,15,16,43,50,51]:

$$P_v = \left[\frac{NDVI - NDVI_{minimum}}{NDVI_{maximum} - NDVI_{minimum}}\right]^2, \quad (9)$$

where P_v is the proportion of vegetation and $NDVI$ (calculated using Equation (11) (see Section 2.5)).

Before the calculation of NDVI, reflectance values were extracted from red band and near infrared (NIR) band using Equation (10) [47]:

$$\rho^{\varphi} = M_{\rho} Q_{Cal} + A_{Q}, \tag{10}$$

where ρ^{φ} is TOA reflectance, which is devoid of correction of the solar angle, M_{ρ} is the multiplicative rescaling factor based on a specific band from the metadata, Q_{Cal} is the quantized and calibrated pixel values (digital number (DN)) of the standard product, and A_{Q} is the additive rescaling factor based on a specific band from the metadata.

Finally, to obtain the value of LST in Celsius (°C), Equation (11) was incorporated [15,51]:

$$LST = LST(K) - 273.15. \tag{11}$$

2.5. NDVI Computation

NDVI is one of the major indicators to understand the urban climate [4]. It ranges between −1 and +1, where large positive values denote vegetation, small positive values denote built-up or bare soils, and negative to adjacent to negative values denote water bodies [39]. It provides information about vegetation abundance, phenology, and health [40]. NDVI was retrieved using Equation (12) through red band and near infrared (NIR) band [15,17]:

$$NDVI = \left[\frac{NIR_{Band} - Red_{Band}}{NIR_{Band} + Red_{Band}}\right], \tag{12}$$

where NIR band represents Band 4 in Landsat TM (0.76–0.90 µm (wavelength)) and Band 5 in Landsat OLI (0.85–0.88 µm (wavelength)) respectively, and RED band represents Band 3 in Landsat TM (0.63–0.69 µm (wavelength)) and Band 4 in Landsat OLI (0.64–0.67 µm (wavelength)), respectively.

2.6. NDBI Computation

NDBI is one of the major indicators to understand the urban climate [4]. It ranges from −1 to +1, where a large positive value denotes the built-up area, a small positive value denotes bare soils, and a negative value denotes water bodies and vegetation [39]. It provides information about the presence and extent of imperviousness [40]. NDBI was retrieved using Equation (13) through NIR band and mid infrared (MIR) [15,17]. Before the calculation of NDBI, reflectance values of NIR band and MIR band were extracted using Equation (10) (Section 2.4):

$$NDBI = \left[\frac{MIR_{Band} - NIR_{Band}}{MIR_{Band} + NIR_{Band}}\right], \tag{13}$$

where MIR band represents Band 5 in Landsat TM (1.55–1.75 µm (wavelength)) and Band 6 in Landsat OLI (1.57–1.65 µm (wavelength)), respectively, and NIR band represents Band 4 in Landsat TM (0.76–0.90 µm (wavelength)) and Band 5 in Landsat OLI (0.85–0.88 µm (wavelength)), respectively.

2.7. Urban–Rural Gradient

The gradient analysis is a useful method to assess the spatial and temporal variation of the environmental variable with the distance [53,54]. This analysis provides information about the spatial pattern of mean LST, NDVI, and NDBI by the urban–rural gradient. It gives notions about the distribution of LST, NDVI, and NDBI from the city center to the city's periphery or suburban area and how it is fluctuating over the landscape of the city [43]. This task was carried out by taking NDVI, NDBI, and LST values from the city center to its periphery at 1 km intervals up to 32 km.

2.8. Statistical Analysis

Based on linear regression, the scattered plot was created for all four time-points, i.e., 1988, 1998, 2008, and 2018 between LST and NDVI and between LST and NDBI. For this task, all pixel values of LST, NDVI, and NDBI were converted into points of data [4]. This task was performed using a total of 0.66 million points in the distinct datasets, i.e., LST, NDVI, and NDBI, for each of the study years (1988, 1998, 2008, and 2018).

3. Results

3.1. Accuracy Assessment Report of LU/LC Classification

Tehran has been classified into five distinct LU/LC classes, i.e., IL, VL, WB, FL, and OL (Table 2). In this analysis, four different time-points (1988, 1998, 2008, and 2018) were taken into consideration to depict the spatial pattern of LU/LC dynamics, where user accuracy and producer accuracy have indicated more than 80% in all LU/LC classes. The overall accuracy achieved for all classifications was more than 85%. The Kappa coefficient was 0.841 in 1988, 0.854 in 1998, 0.895 in 2008, and 0.909 in 2018 (Table 3).

Table 2. Delineated classes of land use/land cover (LU/LC) of the metropolitan city of Tehran.

Sl. No.	Class of LU/LC	Description LU/LC Class
1	IL	Impervious Land (Residential, commercial, industrial settlements, parking lots, and transport network)
2	VL	Vegetation Land (Forest-steppe and mixed forests)
3	WB	Water Bodies (Lakes, ponds, reservoirs, and open water)
4	FL	Farm Land (Crop fields and fallow field)
5	OL	Open Land (Abandoned land, barren land, bare land)

Table 3. Report of accuracy assessment on LU/LC classification (1988–2018) in Tehran.

LU/LC Classes		Year			
		1988	1998	2008	2018
User Accuracy	IL	84.0	86.0	90.0	92.0
	VL	86.0	82.0	88.0	90.0
	WB	100.0	98.0	100.0	100.0
	FL	84.0	88.0	88.0	90.0
	OL	82.0	88.0	92.0	92.0
Producer Accuracy	IL	89.4	84.3	90.0	90.2
	VL	91.5	91.0	89.8	91.8
	WB	98.0	96.1	96.2	98.0
	FL	89.7	86.3	89.8	90.0
	OL	82.0	80.0	92.0	92.0
Overall Accuracy		87.2	88.4	91.6	92.8
Kappa Coefficient		0.841	0.854	0.895	0.909

3.2. Spatiotemporal Pattern of LU/LC Dynamics

The spatial LU/LC maps of Tehran are shown in Figure 2. The IL class expanded the most among all classes, as it was 144.72 km^2 in 1988, which increased to 244.50 km^2 in 1998; later, in 2008, it again increased to 343.83 km^2 and, lastly, it again enlarged to 430.77 km^2 in 2018 (Table 4 and Figure 3). This means that 286.04 km^2 (48.27% of total land) of other LU/LC classes were converted into IL class from 1988 to 2018 (Table 5 and Figure 4). The WB class, the least expanded class, was 0.41 km^2 in 1988, which increased to 0.51 km^2 in 1998; later, in 2008, it again increased to 0.60 km^2 and, lastly, it again enlarged to 2.21 km^2 in 2018 (due to an artificially created lake, called Chitgar Lake (Figure 2d) whose work started in September 2010 and where 80% of the water comes from Kan Creek [55]) (Table 4 and Figure 3). This implies that 1.80 km^2 (0.30% of total land) of other LU/LC classes were converted into

WB land class from 1988 to 2018 (Table 5 and Figure 4). The OL class, which shrank the most among all classes, was 316.38 km^2 in 1988 and decreased to 244.50 km^2 in 1998; later, in 2008, it again decreased to 343.83 km^2 and further diminished to 122.54 km^2 in 2018 (Table 4 and Figure 3). The observed changes indicated that 193.84 km^2 (32.71% of total land) of OL were converted into other LU/LC classes (especially into IL) from 1988 to 2018 (Table 5 and Figure 4). The VL class was second in terms of decrease, as it was 72.19 km^2 in 1988, which decreased to 66.80 km^2 in 1998; later, in 2008, it again decreased to 59.47 km^2 and continued to diminish to 30.14 km^2 in 2018 (Table 4 and Figure 3). This means that 42.06 km^2 (7.10% of total land) of VL were converted into other LU/LC classes from 1988 to 2018 (Table 5 and Figure 4). The FL class, the least shrunk among all classes, was 58.93 km^2 in 1988 and decreased to 28.28 km^2 in 1998; later, in 2008, it again decreased to 23.76 km^2, and further diminished to 6.99 km^2 in 2018 (Table 4 and Figure 3). This indicated that 51.94 km^2 (8.76% of total land) of FL were converted into other LU/LC classes from 1988 to 2018 (Table 5 and Figure 4).

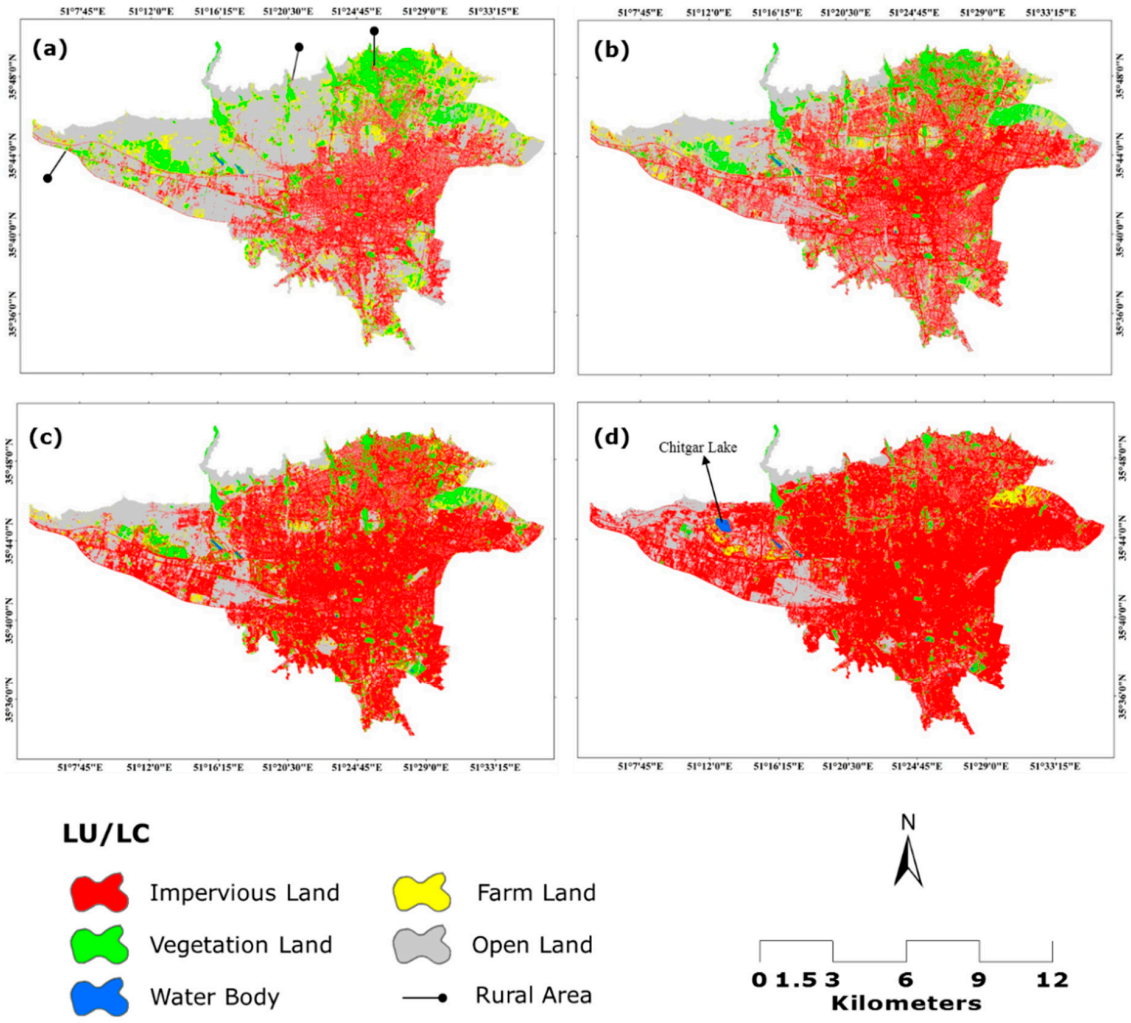

Figure 2. Spatial LU/LC dynamics in Tehran, (**a**) LU/LC Map of 1988, (**b**) LU/LC Map of 1998, (**c**) LU/LC Map of 2008, and (**d**) LU/LC Map of 2018.

Table 4. LU/LC statistics summary for Tehran from 1988 to 2018 at 10-year intervals.

LU/LC Types	1988		1998		2008		2018	
	km^2	%	km^2	%	km^2	%	km^2	%
IL	144.72	24.42	244.50	41.26	343.83	58.02	430.77	72.69
VL	72.19	12.18	66.80	11.27	59.47	10.04	30.14	5.09
WB	0.41	0.07	0.51	0.09	0.60	0.10	2.21	0.37
FL	58.93	9.94	28.28	4.77	23.76	4.01	6.99	1.18
OL	316.38	53.39	252.55	42.61	164.98	27.84	122.54	20.68
Total	592.64	100.00	592.64	100.00	592.64	100.00	592.64	100.00

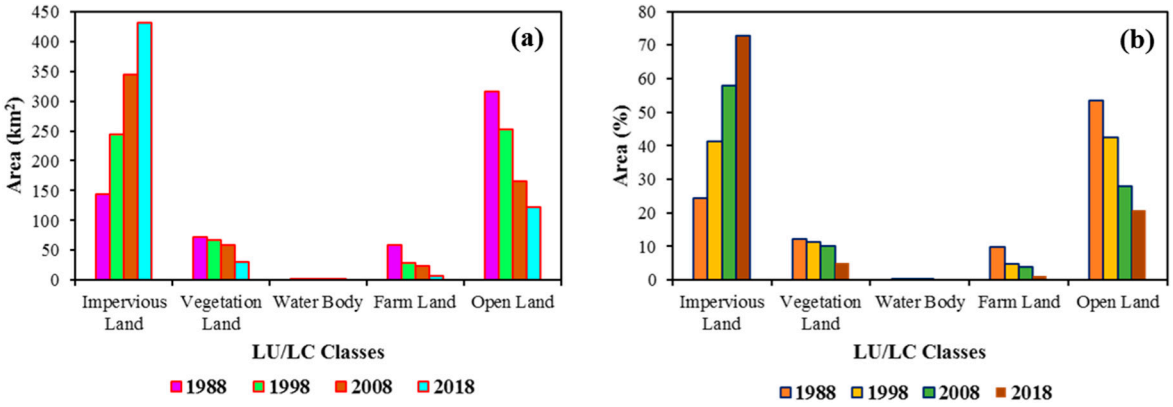

Figure 3. Description of LU/LC statistics of Tehran from 1988 to 2018 at 10-year intervals; (**a**) area (in km^2), and (**b**) area (in percentage (%)).

Table 5. LU/LC change statistics for Tehran from 1988 to 2018 at 10-year intervals.

LU/LC Class	1988–1998		1998–2008		2008–2018		1988–2008		1988–2018		1998–2018	
	km^2	%	km^2	%	km^2	%	km^2	%	km^2	%	km^2	%
IL	−99.8	−16.8	−99.3	−16.8	−86.9	−14.7	−199.1	−33.6	−286.0	−48.3	−186.3	−31.4
VL	5.4	0.9	7.3	1.2	29.3	5.0	12.7	2.2	42.1	7.1	36.7	6.2
WB	−0.1	0.0	−0.1	0.0	−1.6	−0.3	−0.2	0.0	−1.8	−0.3	−1.7	−0.3
FL	30.7	5.2	4.5	0.8	16.8	2.8	35.2	5.9	51.9	8.8	21.3	3.6
OL	63.8	10.8	87.6	14.8	42.4	7.2	151.4	25.6	193.8	32.7	130.0	21.9

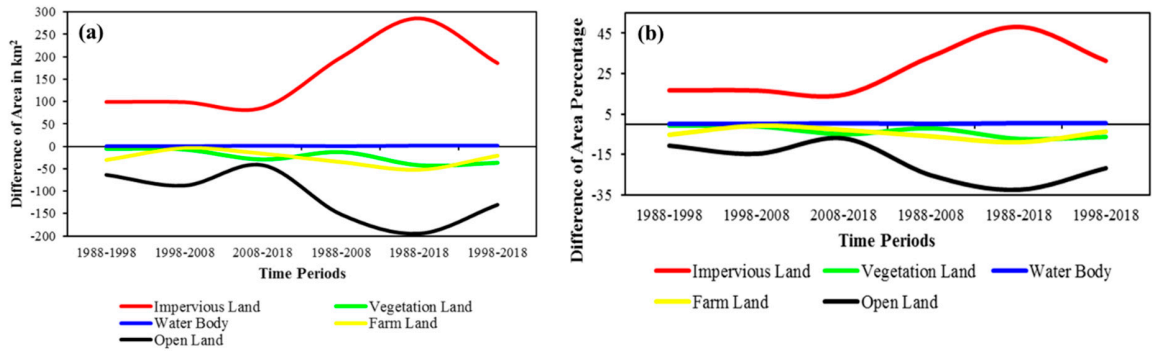

Figure 4. Descriptions of LU/LC class at different time periods in Tehran; (**a**) difference of area (km^2) for each LU/LC class in different time periods, and (**b**) difference of area percentage for each LU/LC class in different time periods.

3.3. Spatiotemporal Pattern of LST Dynamics and Creation of SUHI Phenomena

The SUHI maps of Tehran are shown in Figure 5, where four different time-points (1988, 1998, 2008, and 2018) were taken into consideration to depict the spatial pattern of SUHI distribution, whose statistical information is compiled in Table 6. The highest rise in LST was observed on the

eastern and central part of the city in all years covered by the study (1988–2018). The maximum rise in LST was due to the presence of OL (sandy type) and IL, respectively, whereas the huge decline in LST observed on the northern side of the city was due to the presence of VL (Figure 2).

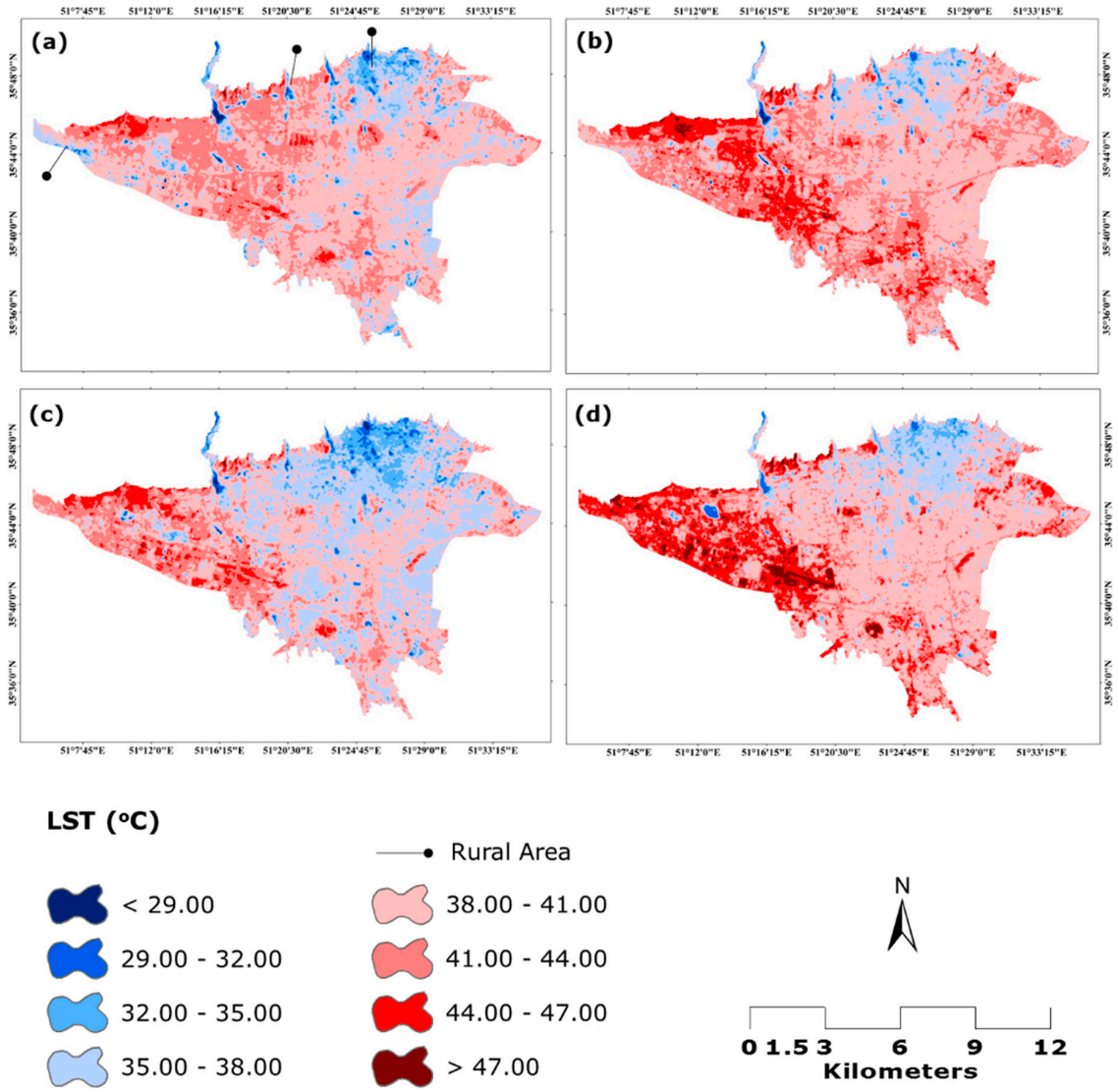

Figure 5. Spatial land surface temperature (LST) dynamics in Tehran, (**a**) LST Map of 1988, (**b**) LST Map of 1998, (**c**) LST Map of 2008, (**d**) LST Map of 2018.

Table 6. Retrieved statistics of LST (°C) values in Tehran of the last three decades at 10-year intervals (1988–2018).

City	Date	Minimum (°C)	Maximum (°C)	Mean (°C)	Standard Deviation
Tehran	17 July 1988	17.81	50.33	39.41	2.54
	21 July 1998	22.94	46.57	37.62	2.70
	1 August 2008	27.25	50.21	38.80	2.94
	12 July 2018	28.92	56.80	40.65	3.19
The difference of Mean LST in Different Time Periods (°C)					
1988–1998	**1998–2008**	**2008–2018**	**1988–2008**	**1988–2018**	**1998–2018**
1.79	−1.18	1.85	0.61	−1.24	−3.03

At the time-point of 1988, rural or suburban areas like south Vardavard (western side of the city), Farahzad (top northwestern side of the city), and Bagh Shater (top northeastern side of the city) (shown in Figures 2 and 5) experienced LST in the range of 29–35 °C, whereas city center areas like North Karoon, Eshrat Abad, and Behjat Abad experienced LST in the range of 38–44 °C (Figure 5). Therefore, it was apparent that the difference of LST was nearly 9–13 °C between rural and urban area, with higher LST in urban than in the rural or suburban areas (Figure 5). Later in the time-points, 1998 and 2008, a 6–9 °C difference in LST was observed, where urban areas recorded LST in the range of 38-44 °C, which was higher than that of rural or suburban areas (in the range of 32–35 °C) (Figure 5). Finally, at the time-point of 2018, the same rural or suburban area faced lower LST (in the range of 35–38 °C) than that of the urban city center area (in the range of 38–44 °C), with a difference of nearly 3–9 °C of LST in the city, except for the rural or suburban area of Vardavard, because it had rapidly developed into an urban area (Figure 2).

3.4. LU/LC Effects on LST

This section describes the mean LST distribution over each distinct LU/LC class to study the dynamic effects of LU/LC on LST. In IL, the mean LST distribution was observed to be 39.30 °C in 1988; later, in 1998, it decreased to 37.70 °C, but in 2008, it increased to 38.47 °C, and in 2018 further increased to 40.38 °C (Table 7). Therefore, it is apparent that the IL class experienced 1.08 °C of higher LST in 2018 in comparison with 1988; however, if the mean LST of the IL class of 2018 is compared with the mean LST of the IL class of 1998, then it experienced 2.68 °C higher mean LST (Table 7). In VL, the distribution of the mean LST was observed to be 35.91 °C in 1988; later, in 1998, it decreased to 34.01 °C, but in 2008, it increased to 35.58 °C, and finally, in 2018, it again increased to 37.18 °C (Table 7). Therefore, it is apparent that the VL class experienced 1.27 °C higher mean LST in 2018 in comparison with the mean LST of VL of 1988, but if the mean LST of VL in 2018 is compared with the mean LST of VL of 1998, then it experienced 3.17 °C higher LST (Table 7). In WB, the mean LST distribution was observed to be 32.87 °C in 1988; later, in 1998, it decreased to 30.53 °C, but in 2008, it increased to 32.52 °C, and finally, in 2018, it again increased to 33.63 °C (Table 7). Therefore, it is evident that WB class experienced 0.76 °C higher LST in 2018 than in 1988, but if the mean LST of WB of 2018 is compared with the mean LST of WB of 1998, then it experienced 3.10 °C higher mean LST (Table 7). In FL, the distribution of mean LST was observed to be 38.97 °C in 1988; later, in 1998, it decreased to 38.65 °C, but in 2008, it increased to 40.11 °C, and finally, in 2018, it again increased to 40.59 °C (Table 7). Therefore, it is apparent that the FL class experienced 1.62 °C of higher LST in 2018 in comparison with the mean LST of FL of 1988, but if the mean LST of FL of 2018 is compared with 1998, then it experienced 1.94 °C of higher mean LST (Table 7). In OL, the mean LST distribution was observed to be 40.36 °C in 1988; later, in 1998, it decreased to 38.41 °C, but in 2008, it increased to 40.50 °C, and finally, in 2018, it again increased to 42.60 °C (Table 7). Therefore, it is evident that the OL class experienced 2.24 °C higher LST in 2018 in comparison with the mean LST of OL of 1988, but if the mean LST of OL of 2018 is compared with 1998, then it experienced 4.19 °C of higher mean LST (Table 7).

Table 7. The mean LST over each distinct LU/LC classes in Tehran from 1988 to 2018.

LU/LC Class	Mean LST (°C)				The difference of Mean LST (°C)					
	1988	1998	2008	2018	1988–1998	1998–2008	2008–2018	1988–2008	1988–2018	1998–2018
IL	39.30	37.70	38.47	40.38	−1.6	0.77	1.91	−0.83	1.08	2.68
VL	35.91	34.01	35.58	37.18	−1.9	1.57	1.6	−0.33	1.27	3.17
WB	32.87	30.53	32.52	33.63	−2.34	1.99	1.11	−0.35	0.76	3.1
FL	38.97	38.65	40.11	40.59	−0.32	1.46	0.48	1.14	1.62	1.94
OL	40.36	38.41	40.50	42.60	−1.95	2.09	2.1	0.14	2.24	4.19

The magnitude of the mean LST based on a cross cover comparison of LU/LC classes was extracted from all time-points, i.e., 1988, 1998, 2008, and 2018, over Tehran (Table 8 and Figure 6).

The mean LST distribution over LU/LC classes was also extracted for the same time period. It was found that IL had a higher mean LST difference than VL by approximately 2.8–3.7 °C and WB by approximately 6.0–7.2 °C at all consecutive time-points, i.e., 1988, 1998, 2008, and 2018 (Table 8 and Figure 6). However, IL was found to have lower mean LST than FL by approximately 0.2–1.6 °C (except in 1998, which had a higher mean LST than FL by 0.3 °C) and OL by approximately 0.7–2.2 °C at all consecutive time-points, i.e., 1988, 1998, 2008, and 2018 (Table 8 and Figure 6). The reason behind the higher mean LST of the FL and OL than IL was the sandy and deserted type of landscape over the city [10,44], which has led to accelerating LST distribution over the FL and OL.

Table 8. The magnitude of mean LST over each distinct LU/LC class in Tehran from 1988 to 2018.

LU/LC Class (Cross Cover Comparison)	Magnitude of Mean LST (°C)			
	1988	1998	2008	2018
IL-VL	3.39	3.69	2.89	3.2
IL-WB	6.43	7.17	5.95	6.75
IL-FL	0.33	−0.95	−1.64	−0.21
IL-OL	−1.06	−0.71	−2.03	−2.22

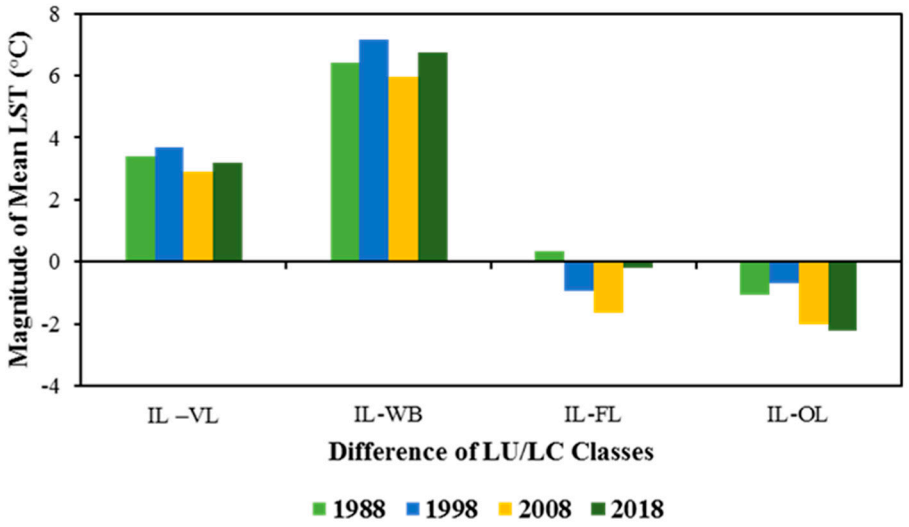

Figure 6. Description of the magnitude of mean LST over each distinct LU/LC class in Tehran from 1988 to 2018.

3.5. Spatiotemporal Pattern of NDVI Dynamics and Its Relationship with LST

The NDVI maps of Tehran are shown in Figure 7, where four different time-points (1988, 1998, 2008, and 2018) take the spatial pattern of NDVI distribution into consideration; their statistical information is portrayed in Table 9. The mean NDVI observed in 1988 was 0.12, which remained the same value in 1998, but after that, the mean NDVI decreased to 0.10 in 2008, then increased to 0.16 in 2018 (Table 9).

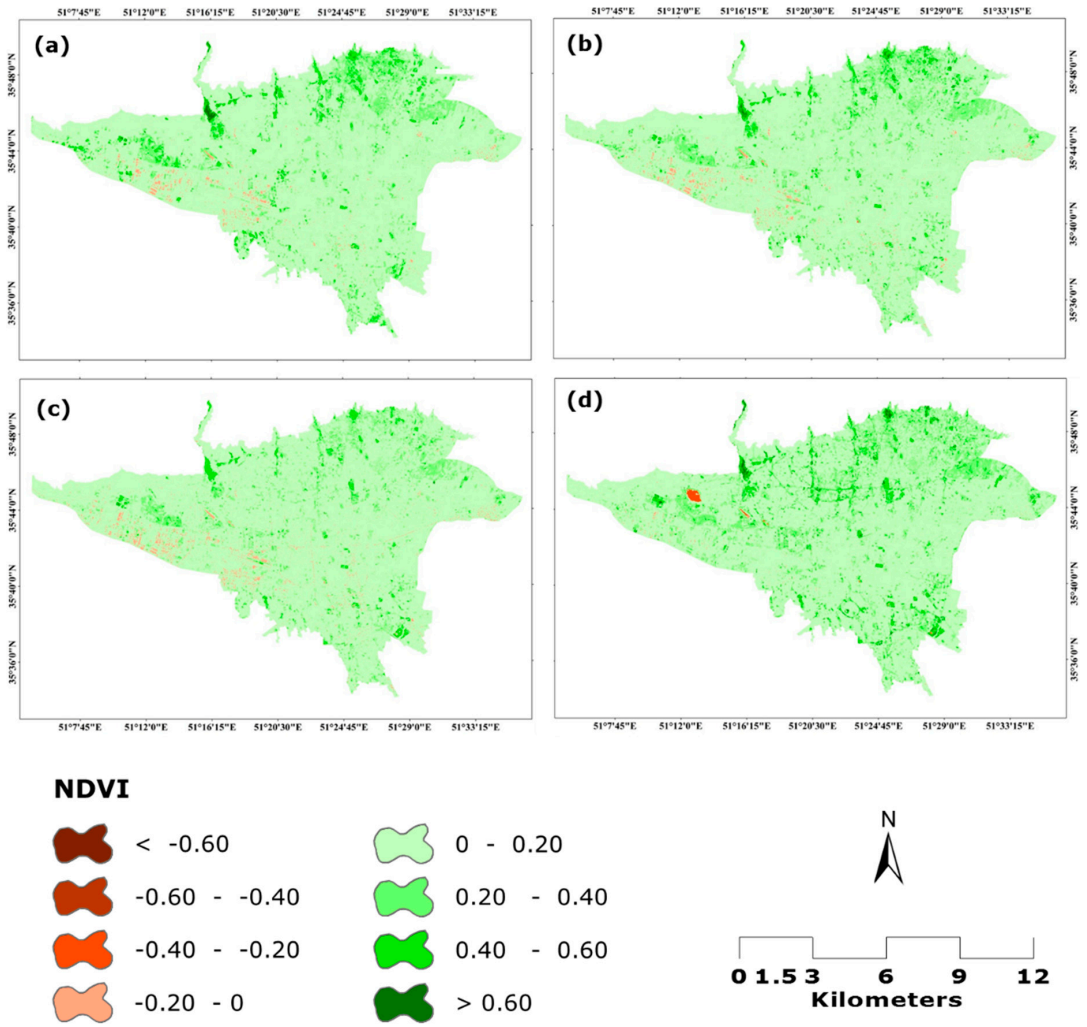

Figure 7. Spatial normal difference vegetation index (NDVI) dynamics in Tehran, (**a**) NDVI Map of 1988, (**b**) NDVI Map of 1998, (**c**) NDVI Map of 2008, and (**d**) NDVI Map of 2018.

Table 9. Retrieved statistics of NDVI values in Tehran.

City	Date	Minimum	Maximum	Mean	Standard Deviation
Tehran	17 July 1988	−0.30	0.74	0.12	0.11
	21 July 1998	−0.77	0.71	0.12	0.10
	1 August 2008	−0.27	0.71	0.10	0.10
	12 July 2018	−0.34	0.76	0.16	0.11

The reason behind the increased amount of mean NDVI of 2018 was the rapid growth of vegetation (grasses and trees) in the parks and gardens in the city (in places like Garden of Turkey's Embassy, Qeytarieh Park, Mellat Park, Laleh Park, City Park of Sangelaj, Azadegan Park, Esfand Park, Tehran Besat Park, Qaem Park, Abrisham Park, Narges Women Park, Nahj Ol-Balagheh Park, Khovardin Garden, Koodak Park, Iran Zamin Park, Aab-o-Atash Park, and Teleghani Park).

The highest distributed NDVI was observed on the northern part and west–central part of the city at all consecutive time-points (1988–2018) due to the presence of dense vegetation; however, in the southern part of the city in 2018, new vegetation has spread, whereas the lowest NDVI has been observed on the eastern and central side of the city due to the presence of OL (sandy land type) and IL, respectively (Figure 7).

The correlation between NDVI and LST was found to be negative at all times, as shown in Figure 5, where the R^2 value dramatically decreased at each time-point, as it was 0.41 in 1988, 0.36 in 1998, 0.23 in 2008, and 0.09 in 2018 (Figure 8). Due to having a negative correlation, it can be stated that the NDVI decreased as LST increased at all time-points, and this relationship showed that due to the presence of lower VL, the LST increased (Table 9). In other words, it can be said that higher VL led to lower LST and lower vegetation led to higher LST (Figure 5).

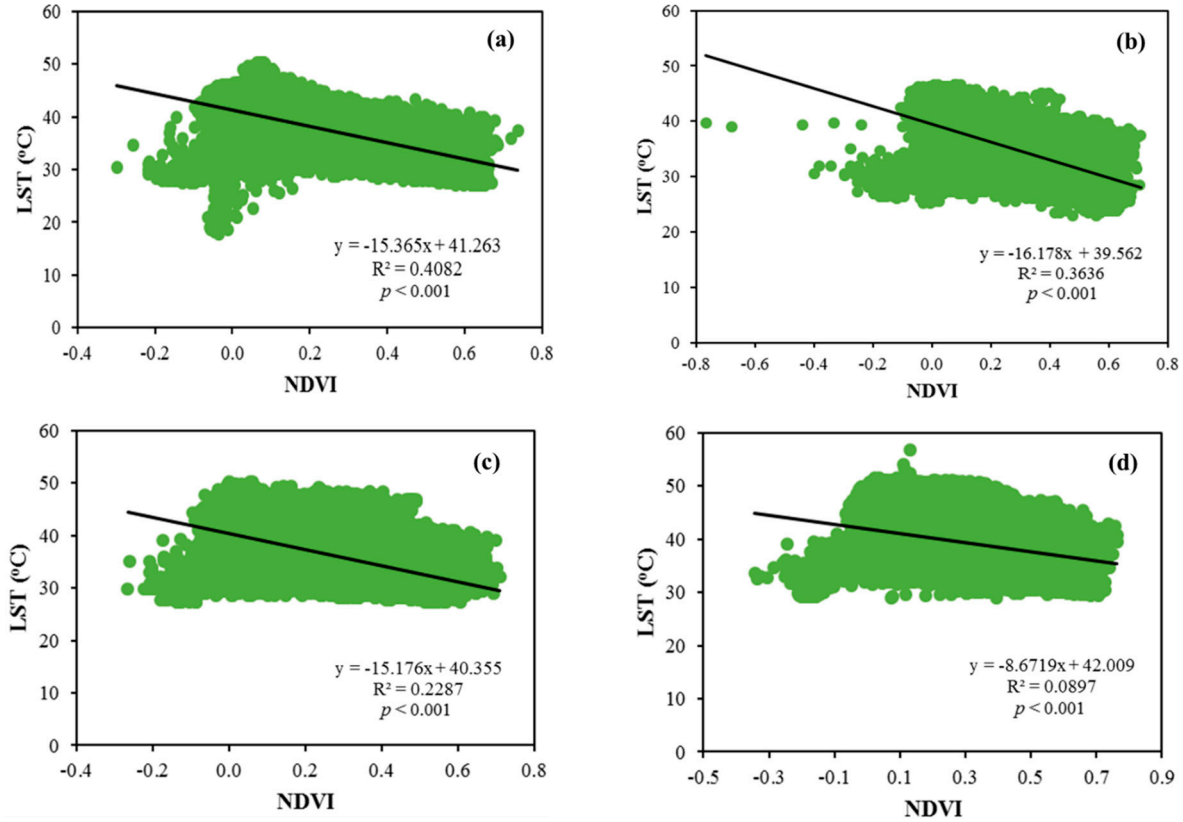

Figure 8. Spatial scattered plots between LST and NDVI in Tehran (1988–2018); (**a**) 1988, (**b**) 1998, (**c**) 2008, and (**d**) 2018.

3.6. Spatiotemporal Pattern of NDBI Dynamics and Its Relationship with LST

The NDBI maps of Tehran are shown in Figure 9, where four different time-points (1988, 1998, 2008, and 2018) were taken into consideration to depict the spatial pattern of NDBI distribution, and their statistical information is shown in Table 10. The mean NDBI was observed to be 0.02 in 1988, and it decreased to 0.01 in 1998, then to −0.01 in 2008, and it remained as the same value in 2018 (Table 10).

The highest distributed NDBI was observed on the western, central, and southern part of the city at all consecutive time-points due to the presence of a dense built-up area with a concrete roadway network, whereas the lowest NDBI was observed on the northern side of the city due to the presence of dense VL (Figure 6).

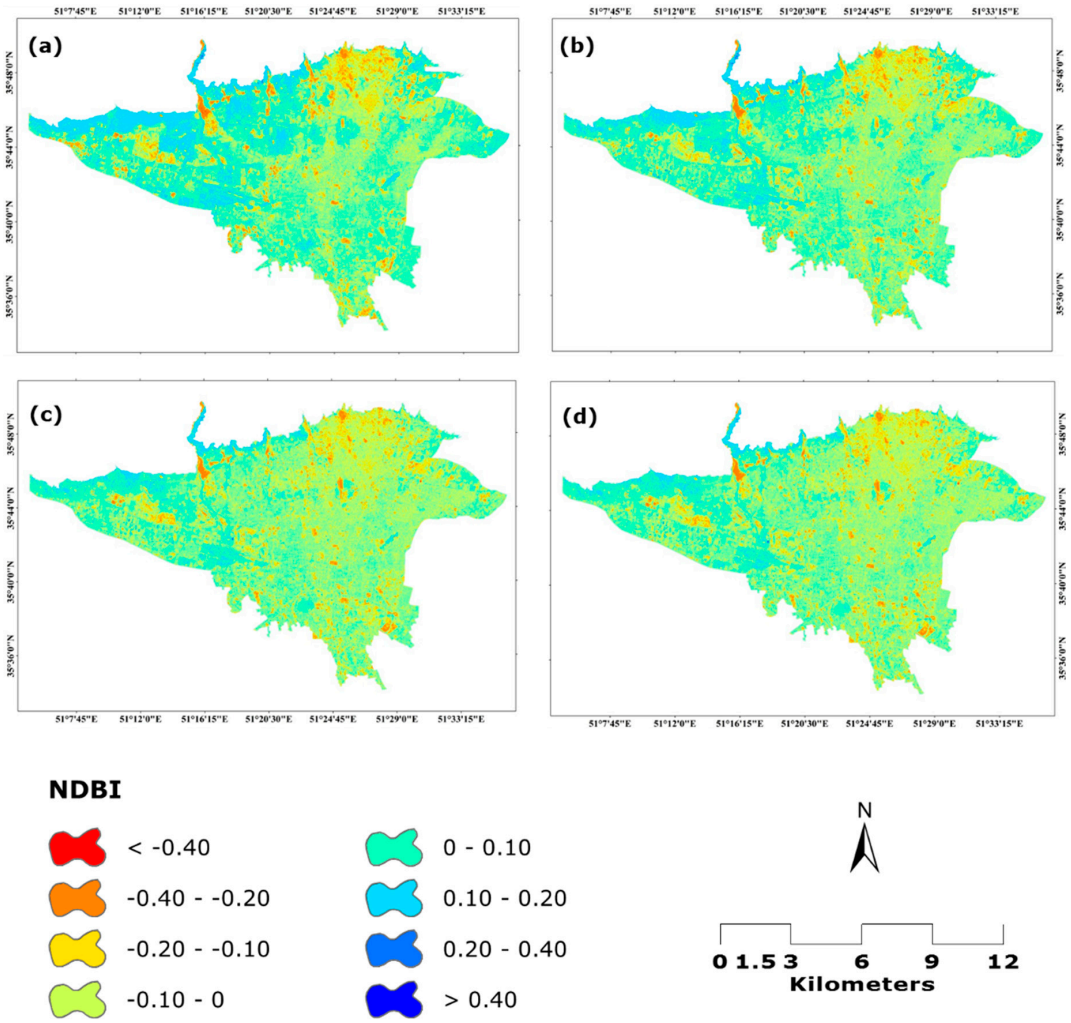

Figure 9. Spatial NDBI dynamics in Tehran; (**a**) NDBI Map of 1988, (**b**) NDBI Map of 1998, (**c**) NDBI Map of 2008, and (**d**) NDBI Map of 2018.

Table 10. Retrieved statistics of normal difference built-up index (NDBI) values in Tehran for the last three decades at 10-year intervals (1988–2018).

City	Date	Minimum	Maximum	Mean	Standard Deviation
Tehran	17 July 1988	−0.43	0.39	0.02	0.08
	21 July 1998	−0.98	0.80	0.01	0.08
	1 August 2008	−0.49	0.35	−0.01	0.07
	12 July 2018	−0.44	0.45	−0.01	0.08

In the context of NDBI effects on LST, the correlation was found to be positive at all times in Figure 10, where the R^2 value dramatically decreased at each time-point, as it was 0.50 in 1988, 0.35 in 1998, 0.34 in 2008, and 0.18 in 2018 (Figure 10). Therefore, due to the increase of both the LST and NDBI, it can be said that IL had strong effects on increasing LST (Table 6), which has been spatially represented in Figure 5.

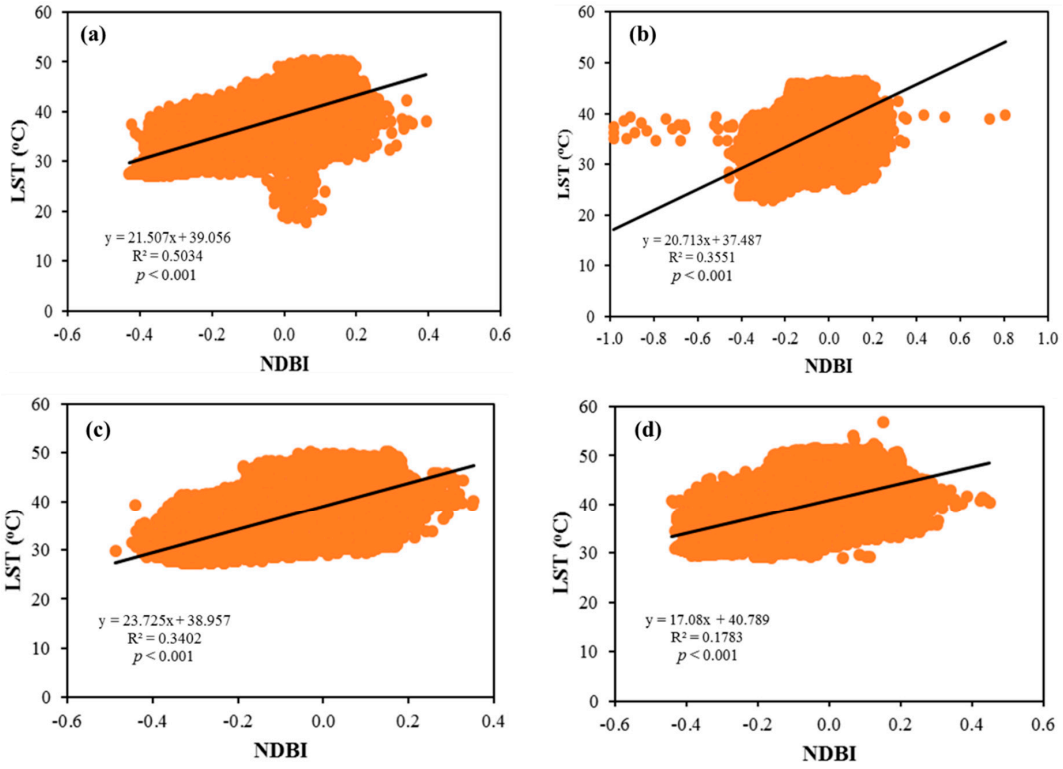

Figure 10. Spatially scattered plots between LST and NDBI in Tehran (1988–2018); (**a**) 1988, (**b**) 1998, (**c**) 2008, and (**d**) 2018.

3.7. Analysis of Pattern of Urban–Rural Gradient

In this Section, the pattern of the urban–rural gradient is described in Figure 11, where the trio relationship among LST, NDVI, and NDBI has been represented at all time-points, i.e., 1988, 1998, 2008, and 2018, respectively, over Tehran. At the first time-point (1988) at the city center, the mean LST was ~38.5 °C with a mean NDVI value of ~0.13 and a mean NDBI value of ~−0.040, and until 15 km, the LST level was 38.5 °C to 40 °C, the mean NDVI level was 0.09 to 0.16, and the mean NDBI level was −0.04 to 0.02. However, after 15 km, the pattern of mean LST and mean NDBI started rising in the range of 38.5 °C to 41 °C and 0.02 to 0.10, respectively, whereas the mean NDVI fell in the range of 0.06 to 0.13 (Figure 11). At the second time-point (1998) at the city center, the mean LST was ~35 °C with a mean NDVI value of ~0.1 and a mean NDBI value of ~−0.035, and until 15 km, the LST level was 36.5 °C to 38 °C, the mean NDVI level was to 0.095 to 0.165, and the mean NDBI level was −0.04 to 0.005. However, after 15 km, the pattern of mean LST and mean NDBI started rising in the range of 37.5 °C to 40.5 °C and −0.01 to 0.09, respectively, whereas the mean NDVI fell in the range of 0.065 to 0.13 (Figure 11). At the third time-point (2008) at the city center, the mean LST was ~38 °C with a mean NDVI value of ~0.11 and a mean NDBI value of ~−0.04, and until 15 km, the LST level was 37 °C to 38.5 °C, the mean NDVI level was 0.075 to 0.14, and the mean NDBI level was −0.04 to −0.01. However, after 15 km, the pattern of mean LST and mean NDBI start rising in the range of 38 °C to 43 °C and −0.015 to 0.075, respectively, whereas the mean NDVI fell in the range of 0.055 to 0.12 (Figure 11). At the fourth and last time-point (2018) at the city center, the mean LST was ~39 °C with a mean NDVI value of ~0.15 and a mean NDBI value of ~−0.02, and until 15 km, the LST level was 39.5 °C to 40 °C, the mean NDVI level was to 0.1 to 0.19, and the mean NDBI level was −0.035 to −0.015. However, after 15 km, the pattern of mean LST and mean NDBI started rising in the range of 37.5 °C to 43 °C and −0.025 to 0.085, respectively, whereas the mean NDVI fell in the range of 0.125 to 0.185 (Figure 11).

Therefore, it is pretty clear that mean LST is dramatically higher in the area of 15 km to 32 km from the city center than in the area of the city center to 15 km, and the mean NDBI value is also higher in the area of 15 km to 32 km from the city center than in the area in city center to 15 km (Figure 11). However, the pattern of mean NDVI has captured the opposite, as the mean NDVI value is lower in the area of 15 km to 32 km from the city center than in the area in the city center to 15 km (Figure 11) at all four consecutive time-points, i.e., 1988, 1998, 2008, and 2018, respectively. Thus, it can be said that the high VL growth led to decreasing LST and high IL growth led to increasing LST.

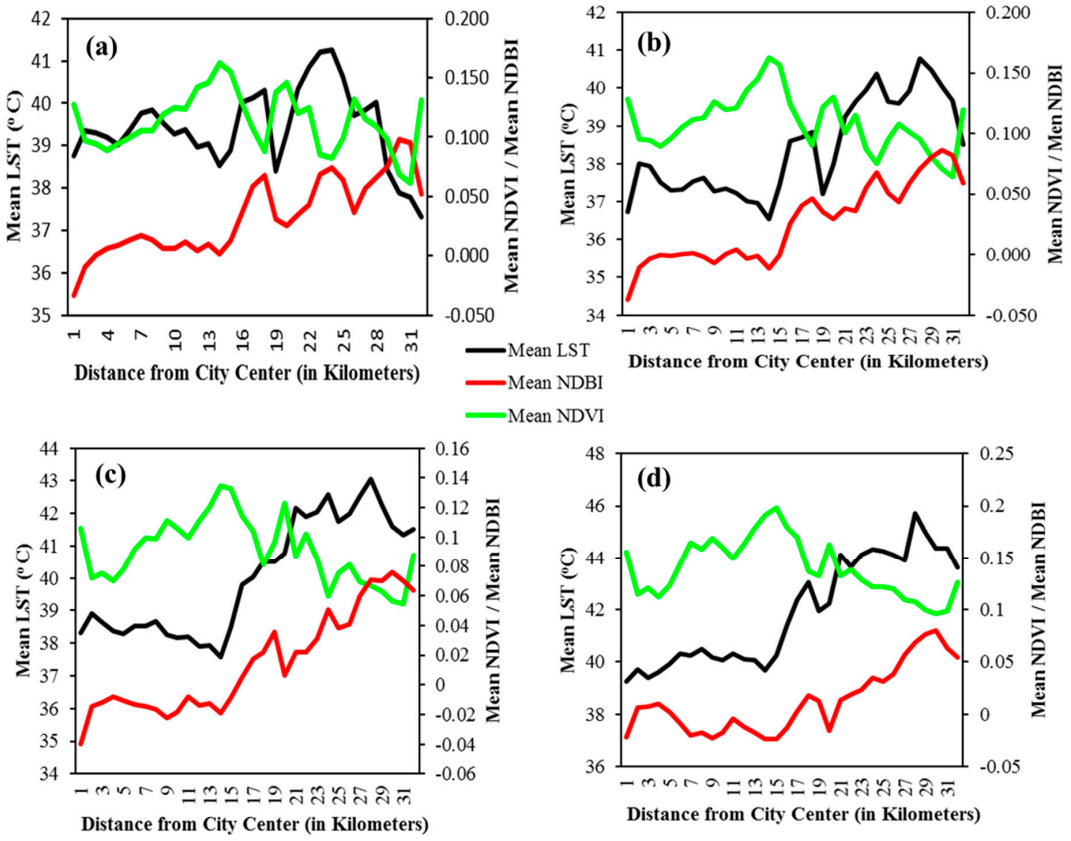

Figure 11. Spatial distribution of urban–rural gradient of LST, NDVI, and NDBI in Tehran (1988–2018); (**a**) 1988, (**b**) 1998, (**c**) 2008, and (**d**) 2018.

4. Discussion

4.1. Urbanization: An Alteration of LU/LC and Its Intensification on LST

The city of Tehran is the capital of Iran and has one of the oldest histories of civilization [10,44]. The city has two major types of physiology: It is mountainous in the northern part and has a desert in the southern part [10,45,46,56]. As this city has a history of human attraction to its landscape, in the course of time, the city has experienced explosive impervious development in the form of residential, commercial, industrial, transport network, parking lots, etc., at the cost of transformation of LU/LC classes like VL, FL, and OL. This trend of alteration in LU/LC dynamics has changed the scenario of the distribution of the LST at a great scale [16,40,57]. One of the major reasons behind all this transformation is the explosive escalation of population growth over a period of time, especially in last three decades, where its human population has grown by nearly 3 million (Figure 12), with their massive demands of land for the growth of their housing, health care, education, creational activities, parking lots, roadways, and others [4,18,58]. A similar kind of transformation has been captured due to the rapid development of built-up land in different parts of the world, like in the city of Baguio in the Philippines [58], the city of Kandy City in Sri Lanka [54], the city of Chennai in India [59],

the metropolitan area of Tokyo in Japan [2], the city of Istanbul in Turkey [60], the city of Mekelle in Ethiopia [61], the municipality of Sobotka in Poland [34], Santiago de Chile [62], São José dos Campos in Brazil [63], and Eastern Europe (Five selected cities in Warsaw, Budapest, Prague, Bucharest, and Sofia) [64].

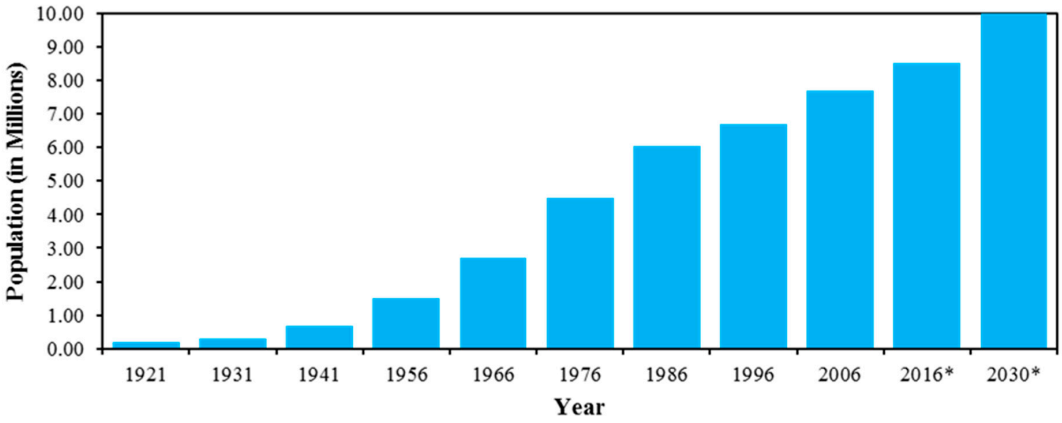

Figure 12. Population of Tehran (1921–2030); Source: Population numbers from 1921 to 2006 have been taken from Roshan et al., 2009 and the population of 2016 and 2030 have been taken from * Data Booklet, 'World's Cities in 2016', 2016.

In this analysis, it has been found that IL very abruptly expanded on the northern side (especially in Chizar, Dezashib, Niavaran, Tajrish, Elahiyeh, Velenjak, Nakhjavan, Ozgol, Shahrak-e-Mahallati, Jafar Abad, Sadat Abad, Farahzad, North Shahran, etc.), southern side (especially in Madreseh, Dolat Abad, Golshahr, Golha, Shahrak-e-Modarres, Azim Abad, Kuy-e-Eslam, Alaein, Karevan, Masoodeih, Lower and Upper Afsariyeh, etc.), and western side (Verdavard, Souht Chitgar, Tehran University Town, Azad Shahr, East and West Golestan, Shahr-e-Ziba, Sharif Town, Shahid Kharazi Town) of the city at each 10-year interval of time-points (Figure 2). By observing the above expansion of land, it could be said that more and more settlement will be built up due to the hectic population pressure, as the United Nations has already published that in 2030, the population of Tehran will be 9.9 million (Figure 12) [1]. Therefore, there is a chance of encroachment in the northern and western part of the city, as in these directions, there is availability of open space.

Therefore, it is apparent that this massive transformation has already enlarged the LST level, as, on the one hand, it was observed that IL, FL, and OL have produced higher LST (nearly 5–7 °C) than vegetation and water body (Figure 13), whereas, on the other hand, in the context of period analysis of LU/LC classes mean LST, IL experienced increased mean LST by 1.08 °C in 1988–2018, and 2.68 °C 1998–2018; VL experienced increased mean LST by 1.27 °C in 1988–2018 and 3.17 °C in 1998–2018; WB experienced increased mean LST by 0.76 °C in 1988–2018 and 3.10 °C in 1998–2018; FL experienced increased mean LST by 1.62 °C in 1988-2018 and 1.94 °C in 1998–2018; and OL experienced increased mean LST by 2.24 °C in 1988–2018 and 4.19 °C 1998–2018 (Table 7 and Figure 14). Mean LST decreased in the period of 1988–1998 in all LU/LC classes, i.e., IL by 1.6 °C, VL by 1.9 °C, WB by 2.34 °C, FL by 0.32 °C, and OL by 1.95 °C (Figure 14); however, in the time period of 1988–2008, a decreasing mean LST was observed in some LU/LC classes, like IL by 0.83 °C, VL by 0.33 °C, WB by 0.35 °C (Figure 14).

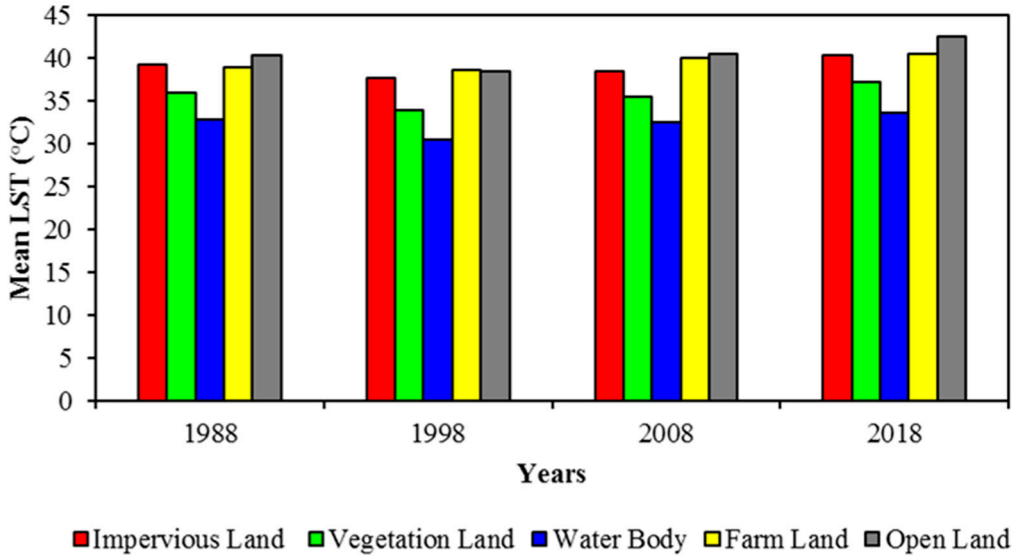

Figure 13. Distribution of Mean LST (°C) over each distinct LU/LC class at different time-points in Tehran.

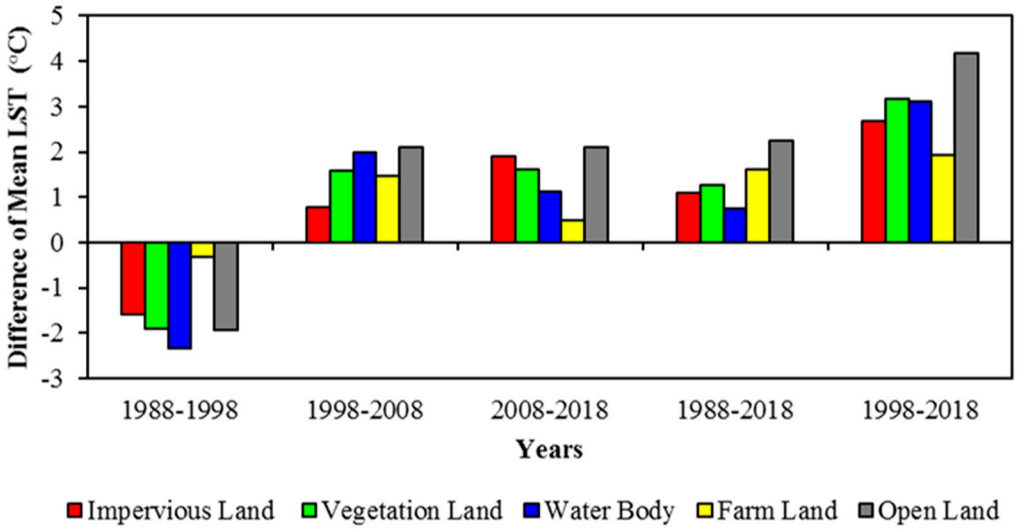

Figure 14. Difference of mean of LST distribution (°C) over each distinct LU/LC class at different time-points in Tehran.

4.2. SUHI Phenomena and Sustainable Planning

In this study, one of the significant observations was the swift enlargement of concrete land (Figure 2) and associated intensification of SUHI effects at a large scale with consistency (Figure 5). The replacement of VL and OL into IL in the form of residential, commercial, industrial, transport network, pavements, parking lots, etc. has consistently occurred on the landscape of the city due to urbanization [4,10]. In this analysis, following LU/LC class-wise mean LST calculation, it has been observed that VL and WB experienced approximately 3–5 °C and 5–8 °C, respectively, lower mean LST compared to other classes (IL, OL, and FL) (Tables 7 and 8). At the time-point of 1998, the observed mean LST distribution was lower than the previous time-point, 1988, over the whole city, but after 1998, the trend of mean LST started increasing at time-points 2008 and 2018, and even the mean LST distribution of 2018 became higher than that of 1988 by 1.24 °C. However, if the comparison is between the mean LST of 1998 and 2018, then the mean LST increased by 3.03 °C (Table 6 and Figure 5).

The clear observation of intensification of LST distribution was recognized throughout the city space and this happened because of VL, which was very dramatically diminished, as it was 72.19 km^2

(12.18 % of total area) in 1988, 66.80 km^2 (11.27% of total area) in 1998, 59.47 km^2 (10.04% of total area) in 2008, and 30.14 km^2 (5.09% of total area) in 2018 (Table 4 and Figure 2). Therefore, it was pronounced that 42.06 km^2 (7.10% of total area) of green space were depleted (Table 5). However, in the context of the phenomena of SUHI, people have focused on geometry and design effects on the flow of wind, which include orientation, shape, and size of buildings; and a mitigation strategy, which includes cool roofs, cool pavements, green roofs, and the use of light materials, but the information of spatial recognition of green space pattern in the city is an essential element to enrich the sustaining environment over the city space [4,16,43].

One of the significant observations of this article was the pattern of LST over the city space of Tehran, because in the city center, the mean LST was lower than that in the periphery of the city (Figures 5 and 11) at all time-points, and this was much pronounced in 2008 and 2018. After 10–15 km of the city center, the LST level increased due to an NDBI level hike (as enormous population pressure has been developed primarily from the last 30 years (Figure 12)) and NDVI level decrease. The city of Tehran has experienced an explosive formation of SUHI in the periphery of the city. The reason behind this formation was the dense concrete development (especially in the areas of Tajrish, Elahiyeh, Velenjak, Nakhjavan, Ozgol, Shahrak-e-Mahallati, Verdavard, Sharif Town, Dolat Abad, Golshahr, Golha, Shahrak-e-Modarres, Azim Abad, Kuy-e-Eslam, and Alaein) in the outer part of the city center or periphery of the city at large scale with the destruction of green space (especially in the areas of Dezashib, Chizar, Tazrish, Ealhiyeh, Niavaran, and Kan), and another reason behind it was having sandy (bare land) and deserted forms of open landscapes.

4.3. Implication of Urban Sustainability

Typically, in the main process of urban enlargement, some features have come into existence with economic improvement and social welfare for the people to a great extent, which directly or indirectly transformed the landscape of the city [4,8,30,51,65]. Despite the fact that due to urban development, people have better employment and other enormous chances to boost urban revenue, which spurs the economy, it is also hard to conceive that the devastation of VL and the small size of WB has taken place at a large scale, which is responsible for accelerating the SUHI level that led to the damage of the local environment [4,5,16,39,66–68].

Tehran experienced IL expansion in the central (lower rate) and outer (higher rate) parts of the city from 1988–2018, which has been witnessed in the LU/LC change statistics (Table 4 and Figure 2); such an unbalanced development built-up pattern should be responsible for the formation of the urban jungle.

Therefore, it can be ascertained that the phenomena of SUHI have been escalating at all time-points, except time-point 1998. It is also clear that this has happened due to the enormous demands of huge population numbers, which have created a fast development of IL, which creates adverse effects on the local ecosystem. To make the SUHI phenomena weaker, a particular mitigation strategy needs to be incorporated, like the use of light materials and paints, the creation of the green and cool roofs, tree plantation, home gardens, and the creation of small ponds/lakes, which can make a significant difference to minimizing LST levels [16,39,66]. Thus, it is essential to spread awareness about the SUHI phenomena through local, regional, or national government bodies and other authorities among the people to adopt the remedies to overcome the SUHI effects; it is also essential to conduct scientific planning before any urban or suburban development for proper management of the land for sustainable development of the environment [4,39,43,65].

4.4. Limitation and Future Scope of the Study

In this section, the limitations and future scope of work have been ascertained. The major limitation of this study was the availability of Landsat satellite data for the required time-points, because the data were available only for some particular times for the selected study area. Further, the image should be cloud-free; otherwise, neither the calculation of LST nor the classification of

LU/LC is possible, due to the absence of an actual reflectance digital number (DN). Thus, the selection of cloud-free data was essential to carry out this study.

The computation of LST was lengthy, because it required conversion of spectral radiance, land surface emissivity, NDVI, and proportion of vegetation. Therefore, on the one hand, to make it time-efficient, and on the other hand, to generate cloud-free images based on the surrounding DN values, there is a need to develop a suitable algorithm and methodology, which would be the work of future research. The emerging cities of developing and underdeveloping nations can be observed to delineate the change patterns for sustainable development, which can also be the focus of future studies in the same field.

5. Conclusions

In this article, the spatiotemporal pattern of LU/LC change and their quantification were summarized at four different time-points, i.e., 1988, 1998, 2008, and 2018, for the study area, the metropolitan city of Tehran. The results showed that VL has depleted by 42.06 km^2 (7.10% of total land) and OL by 193.8 km^2 (32.7% of total land), whereas IL expanded by 286.04 km^2 (48.27% of total land) between 1988–2018 (Table 4). IL was enlarged throughout the time periods studied, while VL, OL, and FL shrank (Figure 4).

The mean LST distribution of LU/LC classes: The results indicated that VL and WB experienced lower mean LST by approximately 3–4 °C and approximately 6–8 °C, respectively, than other LU/LC classes at all time-points, i.e., 1988, 1998, 2008, and 2018 (Table 7). In the analysis of the magnitude of mean LST distribution of LU/LC classes, it was observed that IL experienced higher mean LST than VL by approximately 2.8–3.7 °C and WB by approximately 6.0–7.2 °C, respectively, at all consecutive time-points, i.e., 1988, 1998, 2008, and 2018. However, IL showed lower mean LST than FL by approximately 0.2–1.6 °C (except in 1998, which had higher mean LST than FL by 0.3 °C) and OL by approximately 0.7–2.2 °C, respectively, at all consecutive time-points, i.e., 1988, 1998, 2008, and 2018 (Table 8 and Figure 6).

By observing the pattern of mean LST distribution from the city center to the periphery of the city, it can be said that SUHI phenomena dramatically increased (especially in the time-point of 2018), and was enlarged after 15 km from the city center (Figure 11) due to the presence of IL. The mean LST enlarged by approximately 2–3 °C at the city center and 5–7 °C at the periphery from 1988–2018.

The results of the relationship between LST vs. NDVI and LST vs. NDBI showed a negative correlation relationship and positive relationship, respectively (Figures 8 and 10). In the context of LST vs. NDVI, it can be said that a higher NDVI led to lower LST and a lower NDVI led to higher LST, where the depletion of VL had a significant role in the escalation of LST because vegetation can reduce temperature by 4–5 °C more, than other LU/LC classes, except water body (Table 7). On the other hand, as LST vs. NDBI was positive, it can be said that a higher NDBI led to higher LST and a lower NDBI led to lower LST, which revealed that the enlargement of IL played a significant role in the acceleration of LST because IL can increase temperature by approximately 4-8 °C of the mean LST more, than other LU/LC classes, such as vegetation and water body (Table 7).

It was evident that due to the rapid development of IL (in the form of residential, commercial, industrial, transport network, pavements, parking lots, etc.), VL, OL, and FL were rapidly eradicated. As a result, a considerable growth of LST in IL was observed in the past three decadal courses of time at 10-year intervals. The surprising fact was that OL had been the higher magnitude of mean LST than all the other LU/LC classes (Table 8). The previous studies revealed that IL has a higher temperature difference compared to other LU/LC categories, especially in tropical mountain cities like the city of Baguio City in the Philippines [58] and the city of Kandy City in Sri Lanka [54]. Therefore, it is essential to incorporate the quantification of the thermal state for the city, because it has described the scenario of the environment of the city in the context of LU/LC effects on SUHI generation.

Thus, it is evident that the objectives have addressed the real scenario in the context of LU/LC change, SUHI phenomena, and the relationship of NDBI and NDVI with LST in the urban–rural gradient for Tehran from 1988 to 2018, which have enhanced the landscape information at 10-year intervals. On the basis of this article, very effective policies and planning can be designed to cope with the growth of urban space, the depletion of vegetation space, reduction in open space, shrinking of farm space, and elimination of small to medium size water bodies by the implementation of some suggested plans, like the use of light materials and light color paints; green roof space; storage of rainwater in small to medium size ponds through rainwater harvesting; and plantation of trees in open available space at large scales by the active participation of individuals, local to regional organizations, and governmental bodies to minimize the SUHI effects by enriching the LU/LC dynamics.

Author Contributions: I.R. and M.O.S. proposed the topic. The corresponding author, M.O.S., commanded the data processing, analysis, and wrote the manuscript. I.R., R.D.G., H.O., M.R., Y.M., H.Z., and T.D.M. helped to enhance the research design, analysis, and manuscript writing.

Funding: This study was funded by the Original and Innovatory Research Program (2017–2019) of Fudan University.

Acknowledgments: The authors thank the USGS team for providing the Landsat images via https://earthexplorer.usgs.gov/. The authors also thank United Nations for providing the population data in its published handbook, 'The World's City in 2016'. The comments and suggestions of the anonymous reviewers are gratefully acknowledged.

Conflicts of Interest: There is no conflict of interest among authors.

References

1. *The World's Cities in 2016*. T. W. C. in 2016—D. B. (ST/ESA/S.A.), Population Deprtment, Department of Economic and Social Affairs, United Nations. 2016. Available online: http://www.un.org/en/development/desa/population/publications/pdf/urbanization/the_worlds_cities_in_2016_data_booklet.pdf (accessed on 28 August 2018).
2. Wang, R.; Derdouri, A.; Murayama, Y. Spatiotemporal simulation of future land use/cover change scenarios in the Tokyo metropolitan area. *Sustainability* **2018**, *10*, 2056. [CrossRef]
3. Singh, P.; Kikon, N.; Verma, P. Impact of land use change and urbanization on urban heat island in Lucknow city, Central India: A remote sensing based estimate. *Sustain. Cities Soc.* **2017**, *32*, 100–114. [CrossRef]
4. Ranagalage, M.; Estoque, R.C.; Murayama, Y. An urban heat island study of the Colombo metropolitan area, Sri Lanka, based on Landsat data (1997–2017). *ISPRS Int. J. Geo-Inf.* **2017**, *6*, 189. [CrossRef]
5. Ranagalage, M.; Estoque, R.C.; Handayani, H.H.; Zhang, X.; Morimoto, T.; Tadono, T.; Murayama, Y. Relation between urban volume and land surface temperature: A comparative study of planned and traditional cities in Japan. *Sustainability* **2018**, *10*, 2366. [CrossRef]
6. Weng, Q.; Lu, D.; Schubring, J. Estimation of land surface temperature-vegetation abundance relationship for urban heat island studies. *Remote Sens. Environ.* **2004**, *89*, 467–483. [CrossRef]
7. Sharma, R.; Chakraborty, A.; Joshi, P.K. Geospatial quantification and analysis of environmental changes in urbanizing city of Kolkata (India). *Environ. Monit. Assess.* **2015**, *187*, 4206. [CrossRef] [PubMed]
8. Estoque, R.C.; Murayama, Y.; Myint, S.W. Effects of landscape composition and pattern on land surface temperature: An urban heat island study in the megacities of Southeast Asia. *Sci. Total Environ.* **2017**, *577*, 349–359. [CrossRef] [PubMed]
9. Yin, J.; Yin, Z.; Zhong, H.; Xu, S.; Hu, X.; Wang, J.; Wu, J. Monitoring urban expansion and land use/land cover changes of Shanghai metropolitan area during the transitional economy (1979–2009) in China. *Environ. Monit. Assess.* **2011**, *177*, 609–621. [CrossRef] [PubMed]
10. Bokaie, M.; Zarkesh, M.K.; Arasteh, P.D.; Hosseini, A. Assessment of urban heat island based on the relationship between land surface temperature and land use/land cover in Tehran. *Sustain. Cities Soc.* **2016**, *23*, 94–104. [CrossRef]
11. Mirzaei, P.A. Recent challenges in modeling of urban heat island. *Sustain. Cities Soc.* **2015**, *19*, 200–206. [CrossRef]

12. Babazadeh, M.; Kumar, P. Estimation of the urban heat island in local climate change and vulnerability assessment for air quality in Delhi. *Eur. Sci. J.* **2015**, *19*, 55–65.
13. Son, N.T.; Chen, C.F.; Chen, C.R.; Thanh, B.X.; Vuong, T.H. Assessment of urbanization and urban heat islands in Ho Chi Minh city, Vietnam using Landsat data. *Sustain. Cities Soc.* **2017**, *30*, 150–161. [CrossRef]
14. Joshi, R.; Raval, H.; Pathak, M.; Prajapati, S.; Patel, A.; Singh, V.; Kalubarme, M.H. Urban heat island characterization and isotherm mapping using geo-informatics technology in Ahmedabad city, Gujarat state, India. *Int. J. Geosci.* **2015**, *6*, 274–285. [CrossRef]
15. Avdan, U.; Jovanovska, G. Algorithm for automated mapping of land surface temperature using Landsat 8 tatellite data. *J. Sens.* **2016**, *2016*, 1–8. [CrossRef]
16. Rosa, A.; De Oliveira, F.S.; Gomes, A.; Gleriani, J.M.; Gonçalves, W.; Moreira, G.L.; Silva, F.G.; Ricardo, E.; Branco, F.; Moura, M.M.; et al. Spatial and temporal distribution of urban heat islands. *Sci. Total Environ.* **2017**, *605–606*, 946–956.
17. Li, X.; Zhou, Y.; Asrar, G.R.; Imhoff, M.; Li, X. The surface urban heat island response to urban expansion: A panel analysis for the conterminous United States. *Sci. Total Environ.* **2017**, *605–606*, 426–435. [CrossRef] [PubMed]
18. Zhang, X.; Estoque, R.C.; Murayama, Y. An urban heat island study in Nanchang City, China based on land surface temperature and social-ecological variables. *Sustain. Cities Soc.* **2017**, *32*, 557–568. [CrossRef]
19. Gagliano, A.; Detommaso, M.; Nocera, F.; Evola, G. A multi-criteria methodology for comparing the energy and environmental behavior of cool, green and traditional roofs. *Build. Environ.* **2015**, *90*, 71–81. [CrossRef]
20. Chaudhuri, A.S.; Singh, P.; Rai, S.C. Modelling LULC change dynamics and its impact on environment and water security: Geospatial technology based assessment. *Ecol. Environ. Conserv.* **2018**, *24*, 300–306.
21. Yao, R.; Wang, L.; Huang, X.; Guo, X.; Niu, Z.; Liu, H. Investigation of urbanization effects on land surface phenology in northeast China during 2001–2015. *Remote Sens.* **2017**, *9*, 66. [CrossRef]
22. Dewan, A.M.; Yamaguchi, Y. Land use and land cover change in Greater Dhaka, Bangladesh: Using remote sensing to promote sustainable urbanization. *Appl. Geogr.* **2009**, *29*, 390–401. [CrossRef]
23. Ramachandra, T.V.; Kumar, U. Land surface temperature with land cover dynamics: Multi-resolution, rpatio-temporal data analysis of Greater Bangalore. *Int. J. Geoinform.* **2009**, *5*, 43–53.
24. Grover, A.; Singh, R.B. Analysis of urban heat island (UHI) in relation to normalized difference vegetation index (NDVI): A comparative study of Delhi and Mumbai. *Environments* **2015**, *2*, 125–138. [CrossRef]
25. Deb, S.; Kant, Y.; Mitra, D. Assessment of land surface temperature and heat fl uxes over Delhi using remote sensing data. *J. Environ. Manag.* **2013**, *148*, 143–152.
26. Pandey, P.; Kumar, D.; Prakash, A.; Masih, J.; Singh, M.; Kumar, S.; Jain, V.K.; Kumar, K. A study of urban heat island and its association with particulate matter during winter months over Delhi. *Sci. Total Environ.* **2012**, *414*, 494–507. [CrossRef] [PubMed]
27. Ku, D.N.; Sandeep, N.; Jyothi, S.; Madhu, T. Significant changes on land use/land cover by using remote sensing and GIS analysis-review. *Int. J. Eng. Sci. Comput.* **2017**, *7*, 5433–5435.
28. Gould, W.A.; Gonz, O.M.R. Land development, land use, and urban sprawl in Puerto Rico integrating remote sensing and population census data. *Landsc. Urban Plan.* **2007**, *79*, 288–297.
29. Kuang, W.; Liu, Y.; Dou, Y.; Chi, W.; Chen, G. What are hot and what are not in an urban landscape: Quantifying and explaining the land surface temperature pattern in Beijing, China. *Landsc. Ecol.* **2015**, *30*, 357–373. [CrossRef]
30. Zhang, Y.; Su, Z.; Li, G.; Zhuo, Y.; Xu, Z. Spatial-temporal evolution of sustainable urbanization development: A perspective of the coupling coordination development based on population, industry, and built-up land spatial agglomeration. *Sustainability* **2018**, *10*, 1766. [CrossRef]
31. Rahman, M.T.; Aldosary, A.S.; Mortoja, G. Modeling future land cover changes and their effects on the land surface temperatures in the Saudi Arabian eastern coastal city of Dammam. *Land* **2017**, *6*, 36. [CrossRef]
32. Rahman, M.T. Detection of land use/land cover changes and urban sprawl in Al-Khobar, Saudi Arabia: An analysis of multi-temporal remote sensing data. *ISPRS Int. J. Geo-Inf.* **2016**, *5*, 15. [CrossRef]
33. Krajewski, P.; Solecka, I.; Cetera, B.M. Landscape Change Index as a Tool for Spatial Analysis. *IOP Conf. Ser. Mater. Sci. Eng.* **2017**, *245*, 072014. [CrossRef]
34. Krajewski, P. Assessing change in a high-value landscape: Case study of the municipality of Sobotka, Poland. *Pol. J. Environ. Stud.* **2017**, *26*, 2603–2610. [CrossRef]

35. Kumar, S.; Panwar, M. Urban heat island footprint mapping of Delhi using remote sensing. *Int. J. Emerg. Technol.* **2017**, *8*, 80–83.
36. Agarwal, R.; Sharma, U.; Taxak, A. Remote sensing based assessment of urban heat island phenomenon in Nagpur metropolitan area. *Int. J. Inf. Comput. Technol.* **2014**, *4*, 1069–1074.
37. Mukherjee, S.; Joshi, P.K.; Garg, R.D. Analysis of urban built-up areas and surface urban heat island using downscaled MODIS derived land surface temperature data. *Geocarto Int.* **2017**, *32*, 900–918. [CrossRef]
38. Lee, L.; Chen, L.; Wang, X.; Zhao, J. Use of Landsat TM/ETM+ data to analyze urban heat island and its relationship with land use/cover change. In Proceedings of the 2011 International Conference on Remote Sensing, Environment and Transportation Engineering, Nanjing, China, 24–26 June2011; pp. 922–927.
39. Ranagalage, M.; Estoque, R.C.; Zhang, X.; Murayama, Y. Spatial changes of urban heat island formation in the Colombo district, Sri Lanka: Implications for sustainability planning. *Sustainability* **2018**, *10*, 1367. [CrossRef]
40. Pal, S.; Ziaul, S. Detection of land use and land cover change and land surface temperature in English Bazar urban centre. *Egypt. J. Remote Sens. Space Sci.* **2017**, *20*, 125–145. [CrossRef]
41. Zhang, Y.; Odeh, I.O.A.; Han, C. Bi-temporal characterization of land surface temperature in relation to impervious surface area, NDVI and NDBI, using a sub-pixel image analysis. *Int. J. Appl. Earth Obs. Geoinf.* **2009**, *11*, 256–264. [CrossRef]
42. Thapa, R.B.; Murayama, Y. Drivers of urban growth in the Kathmandu valley, Nepal: Examining the efficacy of the analytic hierarchy process. *Appl. Geogr.* **2010**, *30*, 70–83. [CrossRef]
43. Estoque, R.C.; Pontius, R.G.; Murayama, Y.; Hou, H.; Thapa, R.B.; Lasco, R.D.; Villar, M.A. Simultaneous comparison and assessment of eight remotely sensed maps of Philippine forests. *Int. J. Appl. Earth Obs. Geoinf.* **2018**, *67*, 123–134. [CrossRef]
44. Roshan, G.; Rousta, I.; Ramesh, M. Studying the effects of urban sprawl of metropolis on tourism-climate index oscillation: A case study of Tehran city. *J. Geogr. Reg. Plan.* **2009**, *2*, 310–321.
45. Habibi, R.; Alesheikh, A.A. An assessment of spatial pattern characterization of air pollution: A case study of CO and PM2.5 in Tehran, Iran. *ISPRS Int. J. Geo-Inform.* **2017**, *6*, 270. [CrossRef]
46. Hasanlou, M.; Mostofi, N. Investigating urban heat island estimation and relation between various land cover indices in Tehran city using Landsat 8 imagery. In Proceedings of the 1st International Electronic Conference on Remote Sensing, Basel, Switzerland, 22 June–5 July 2015; pp. 1–11.
47. *Landsat 8 (L8) Data Users Handbook*; version 2; United States Geological Survey: Sioux Falls, SD, USA, 2016; Volume 8.
48. *Landsat 8 (L8) Level 1 (L1) Data Format Control Book (Dfcb)*; version 10; United States Geological Survey: Sioux Falls, SD, USA, 2018; Volume 8.
49. Sexton, J.O.; Urban, D.L.; Donohue, M.J.; Song, C. Long-term land cover dynamics by multi-temporal classi fi cation across the Landsat-5 record. *Remote Sens. Environ.* **2013**, *128*, 246–258. [CrossRef]
50. Ziaul, S.; Pal, S. Image based surface temperature extraction and trend detection in an urban area of West Bengal, India. *J. Environ. Geogr.* **2016**, *9*, 13–25. [CrossRef]
51. Sultana, S.; Satyanarayana, A.N.V. Urban heat island intensity during winter over metropolitan cities of India using remote-sensing techniques: Impact of urbanization. *Int. J. Remote Sens.* **2018**, *39*, 6692–6730. [CrossRef]
52. Ishtiaque, A.; Shrestha, M.; Chhetri, N. Rapid urban growth in the Kathmandu valley, Nepal: Monitoring land use land cover dynamics of a himalayan city with Landsat imageries. *Environments* **2017**, *4*, 72. [CrossRef]
53. Gunaalan, K.; Ranagalage, M.; Gunarathna, M.H.J.P.; Kumari, M.K.N.; Vithanage, M.; Srivaratharasan, T.; Saravanan, S.; Warnasuriya, T.W.S. Application of geospatial techniques for groundwater quality and availability assessment: A case study in Jaffna Peninsula, Sri Lanka. *ISPRS Int. J. Geo-Inf.* **2018**, *7*, 20. [CrossRef]
54. Ranagalage, M.; Dissanayake, D.; Murayama, Y.; Zhang, X.; Estoque, R.C.; Perera, E.; Morimoto, T. Quantifying surface urban heat island formation in the world heritage tropical mountain city of Sri Lanka. *ISPRS Int. J. Geo-Inf.* **2018**, *7*, 341. [CrossRef]

55. Emam, A.; Zolfagharian, M.; Binazadeh, K.; Deilami, H.A.; Eslaminia, A.; Bayat, J. Construction of Chitgar dam's artificial lake -social and construction of Chitgar dam's artificial lake—Social and environmental impact assessment. In Proceedings of the International Symposium on Appropriate technology to ensure proper Development, Operation and Maintenance of Dams in Developing Countries, Johannesburg, South Africa, 15–20 May 2016; pp. 91–100.
56. Falahatkar, S.; Mousavi, S.M. Spatial and temporal distribution of carbon dioxide gas using GOSAT data over IRAN. *Environ. Monit. Assess.* **2017**, *189*, 1–13. [CrossRef] [PubMed]
57. Li, D.; Sun, T.; Liu, M.; Yang, L.; Wang, L.; Gao, Z. Contrasting responses of urban and rural surface energy budgets to heat waves explain synergies between urban heat islands and heat waves. *Environ. Res. Lett.* **2015**, *10*, 1–10. [CrossRef]
58. Estoque, R.C.; Murayama, Y. Monitoring surface urban heat island formation in a tropical mountain city using Landsat data (1987–2015). *ISPRS J. Photogramm. Remote Sens.* **2017**, *133*, 18–29. [CrossRef]
59. Padmanaban, R.; Bhowmik, A.K.; Cabral, P.; Zamyatin, A.; Almegdadi, O.; Wang, S. Modelling urban sprawl using remotely sensed data: A case study of Chennai city, Tamilnadu. *Entropy* **2017**, *19*, 163. [CrossRef]
60. Nigussie, T.A.; Altunkaynak, A.; Asce, A.M. Modeling urbanization of Istanbul under different scenarios using SLEUTH urban growth model. *J. Urban Plan. Dev.* **2016**, *143*, 1–13. [CrossRef]
61. Fenta, A.A.; Yasuda, H.; Haregeweyn, N.; Belay, S.; Hadush, Z.; Gebremedhin, M.A. The dynamics of urban expansion and land use/land cover changes using remote sensing and spatial metrics: The case of Mekelle City of northern Ethiopia changes using remote sensing and spatial metrics: The case of Mekelle City of northern Ethiopia. *Int. J. Remote Sens.* **2017**, *38*, 4107–4129. [CrossRef]
62. García-Ayllón, S. Rapid development as a factor of imbalance in urban growth of cities in Latin America: A perspective based on territorial indicators. *Habitat Int.* **2016**, *58*, 127–142. [CrossRef]
63. Ogashawara, I.; da Silva Brum Bastos, V. A Quantitative Approach for Analyzing the Relationship between Urban Heat Islands and Land Cover. *Remote Sens.* **2012**, *4*, 3596–3618. [CrossRef]
64. Garcia-Ayllon, S. Urban transformations as indicators of economic change in post-communist Eastern Europe: Territorial diagnosis through five case studies. *Habitat Int.* **2018**, *71*, 29–37. [CrossRef]
65. Rimal, B.; Zhang, L.; Keshtkar, H.; Wang, N.; Lin, Y. Monitoring and modeling of spatiotemporal urban expansion and Land-Use/Land-Cover change using integrated Markov Chain Cellular Automata Model. *ISPRS Int. J. Geo-Inf.* **2017**, *6*, 288. [CrossRef]
66. Li, J.; Wang, X.; Wang, X.; Ma, W.; Zhang, H. Remote sensing evaluation of urban heat island and its spatial pattern of the Shanghai metropolitan area, China. *Ecol. Complex.* **2009**, *6*, 413–420. [CrossRef]
67. Xu, R.; Zhang, H.; Lin, H. Annual dynamics of impervious surfaces at city level of Pearl River Delta metropolitan. *Int. J. Remote Sens.* **2018**, *39*, 3537–3555. [CrossRef]
68. Senanayake, I.P.; Welivitiya, W.D.D.P.; Nadeeka, P.M. Remote sensing based analysis of urban heat islands with vegetation cover in Colombo city, Sri Lanka using Landsat-7 ETM+ data. *Urban Clim.* **2013**, *5*, 19–35. [CrossRef]